Cationic Carboxylate and Thioacetate Ruthenium(II) Complexes: Synthesis and Cytotoxic Activity Against Anaplastic Thyroid Cancer Cells

Denise Lovison, Lorenzo Allegri, Federica Baldan, Maurizio Ballico, Giuseppe Damante, Christian Jandl and Walter Baratta

Supporting Information

Table of Contents:

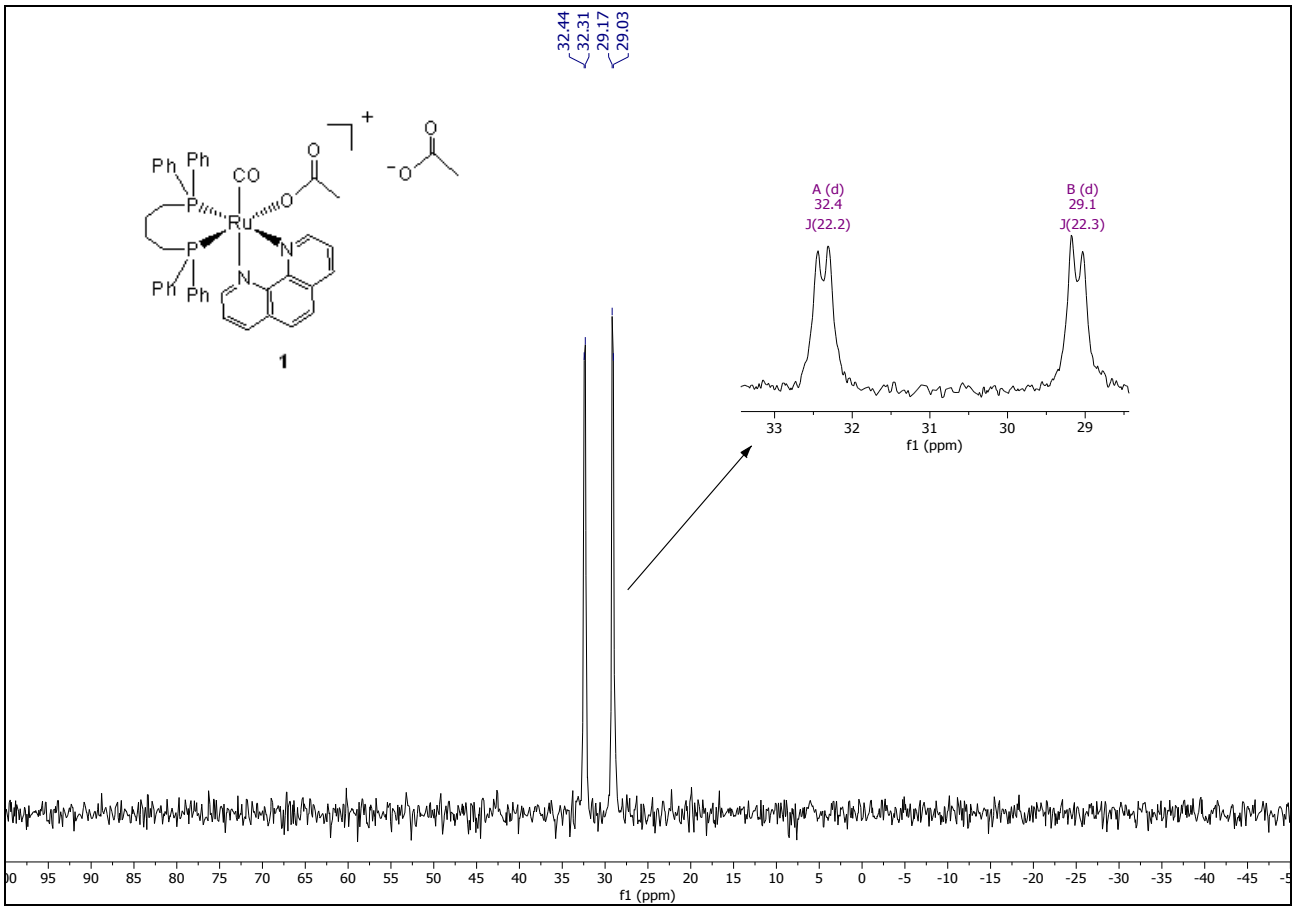

Figure S1. $^{31}P\{^{1}H\}$ NMR spectrum (162 MHz) of [Ru(OAc)(CO)(dppb)(phen)]OAc (**1**) in CD_2Cl_2 at 298 K.

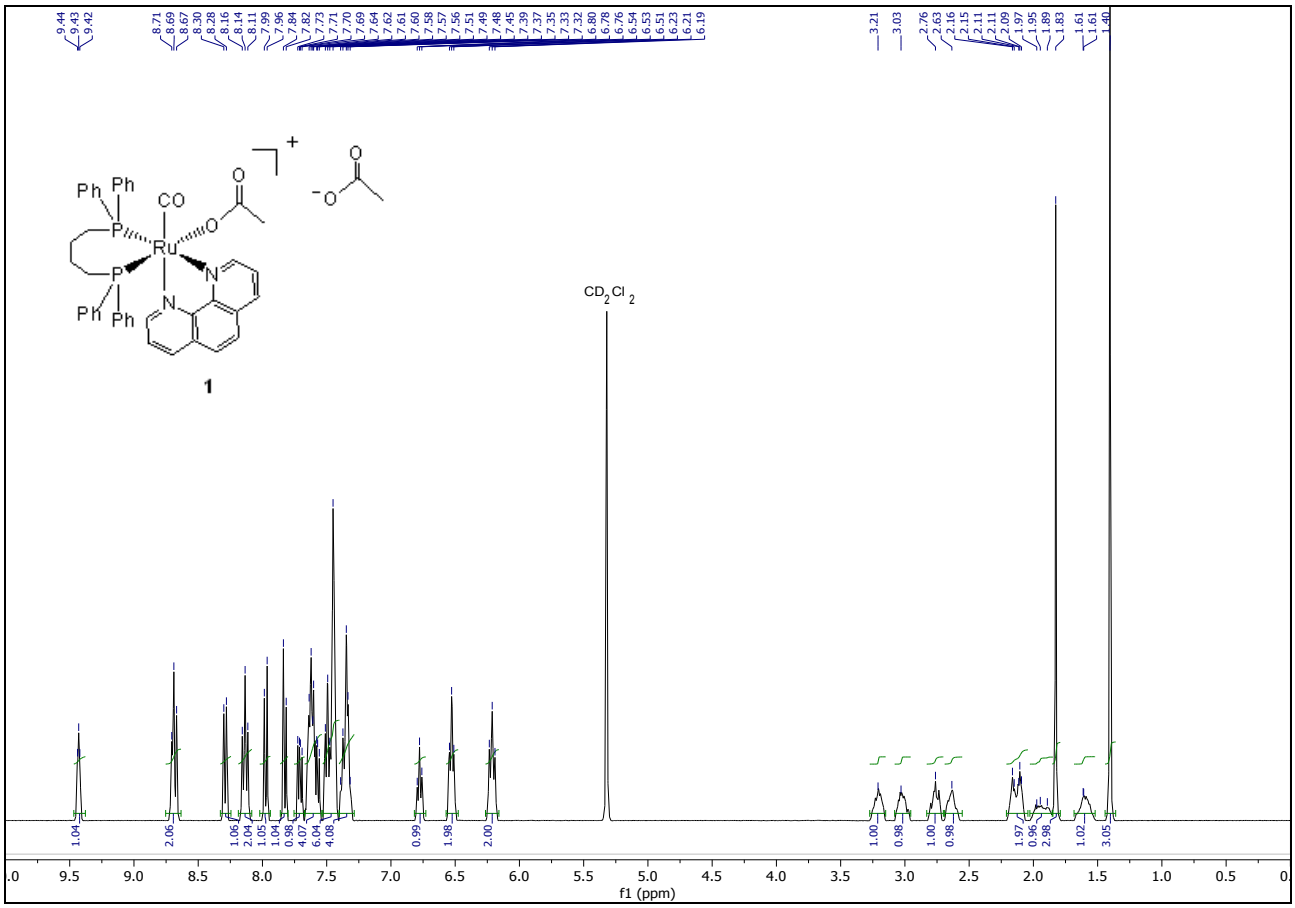

Figure S2. ^{1}H NMR spectrum (400.1 MHz) of [Ru(OAc)(CO)(dppb)(phen)]OAc (**1**) in CD_2Cl_2 at 298 K.

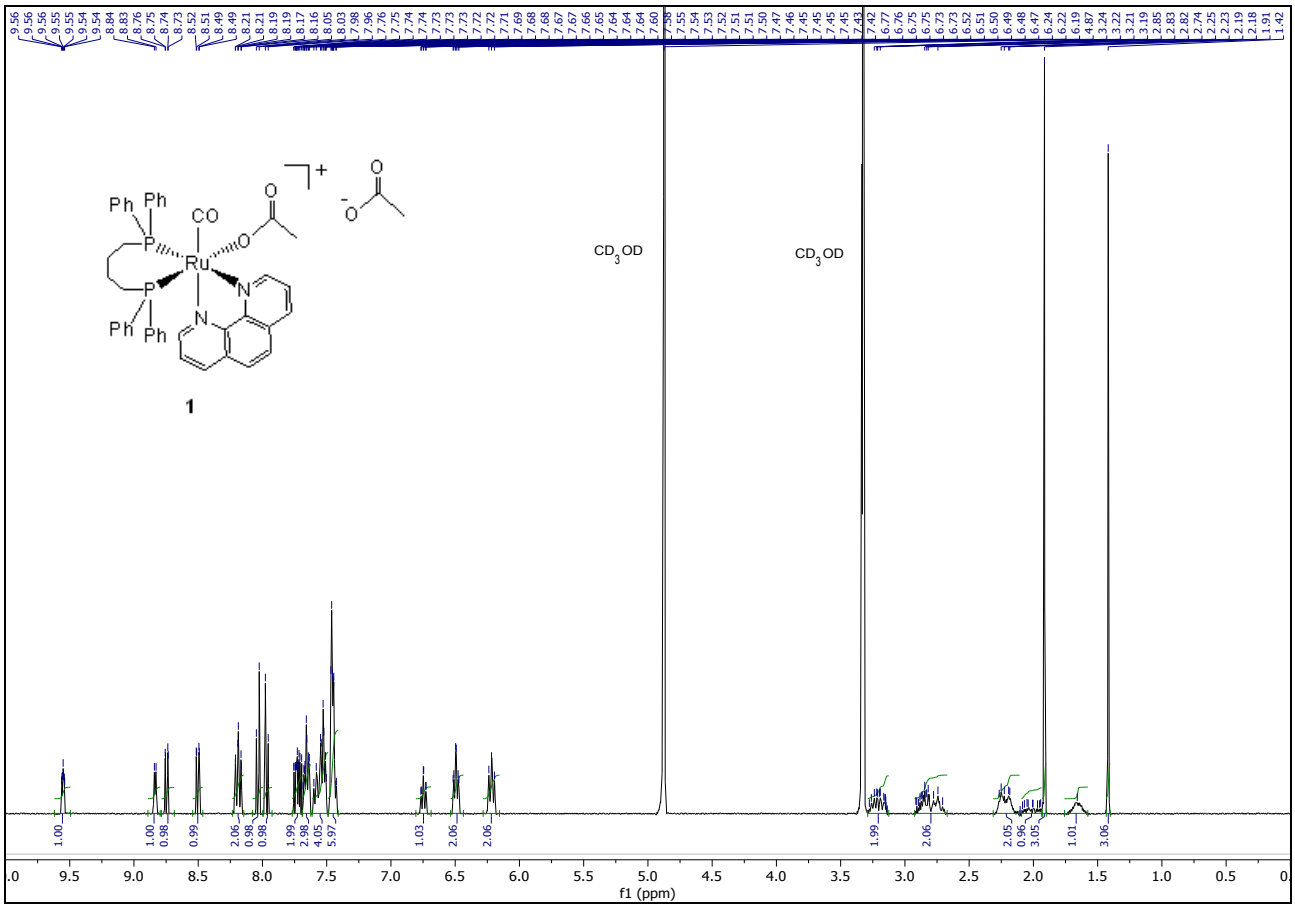

Figure S3. ^{1}H NMR spectrum (400.1 MHz) of [Ru(OAc)(CO)(dppb)(phen)]OAc (**1**) in CD_3OD at 298 K.

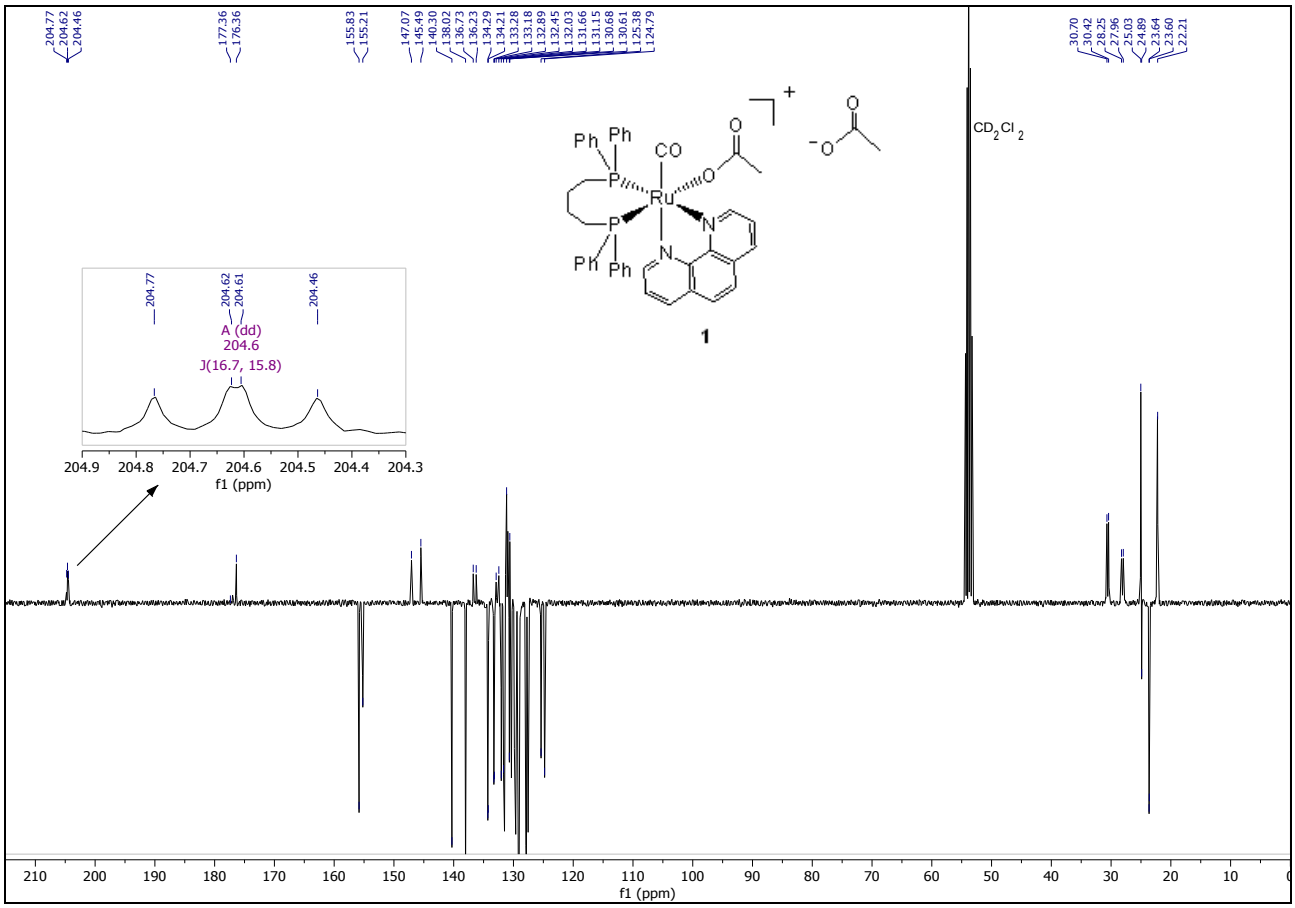

Figure S4. $^{13}C\{^{1}H\}$ DEPTQ NMR spectrum (100.6 MHz) of [Ru(OAc)(CO)(dppb)(phen)]OAc (**1**) in CD_2Cl_2 at 298 K.

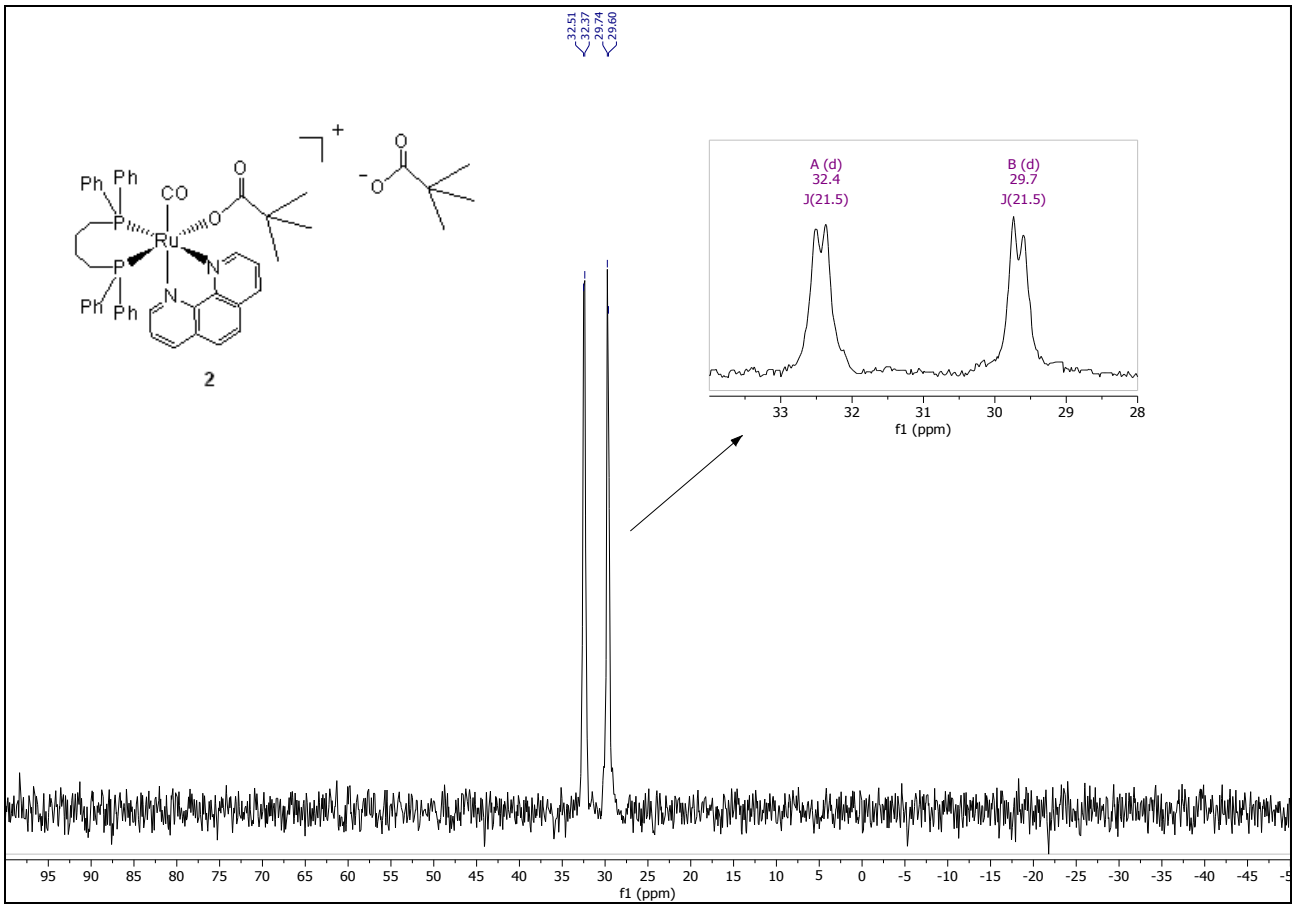

Figure S5. $^{31}P\{^{1}H\}$ NMR spectrum (162 MHz) of [Ru(OPiv)(CO)(dppb)(phen)]OPiv (**2**) in CD_2Cl_2 at 298 K.

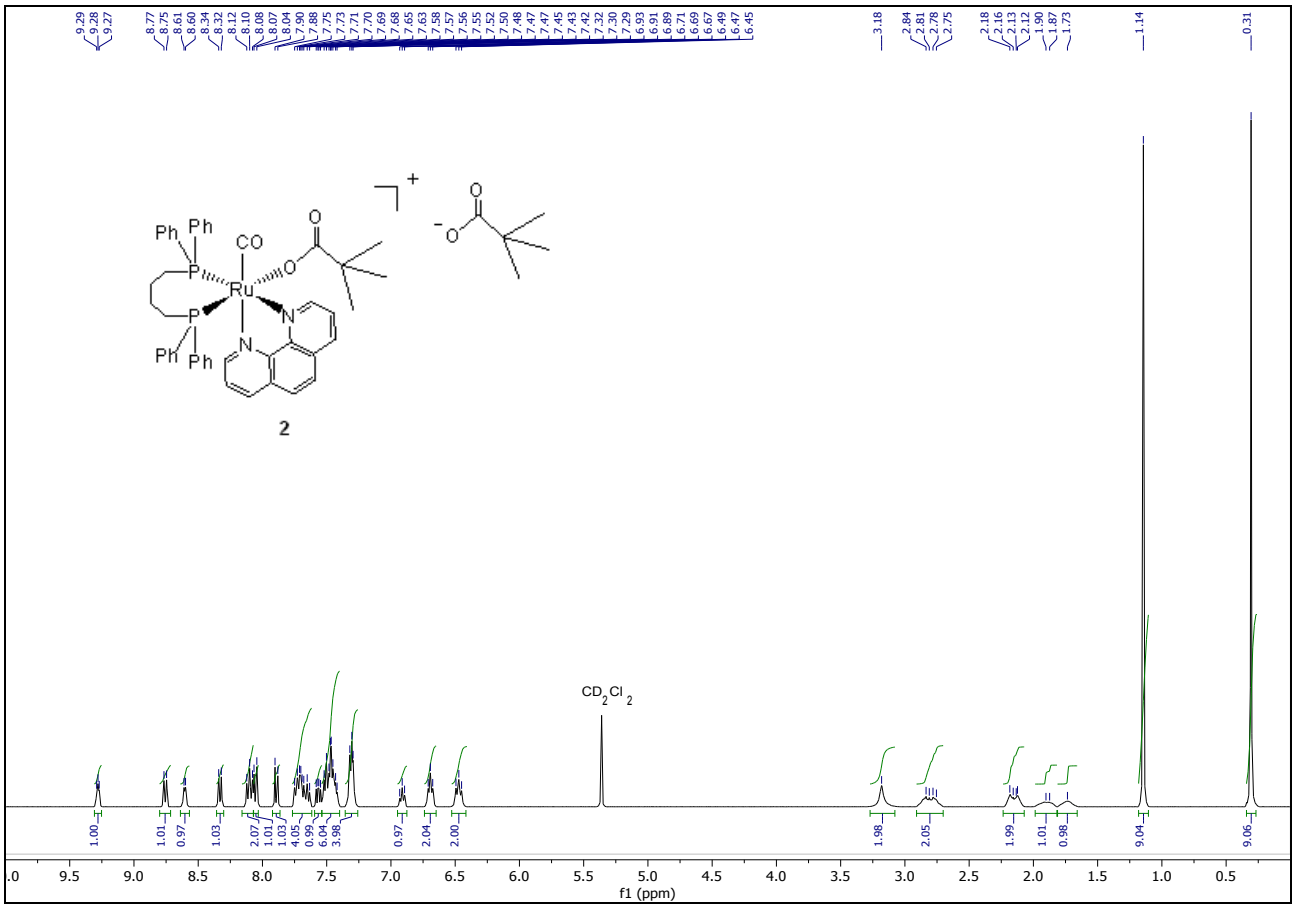

Figure S6. ^{1}H NMR spectrum (400.1 MHz) of [Ru(OPiv)(CO)(dppb)(phen)]OPiv (**2**) in CD_2Cl_2 at 298 K.

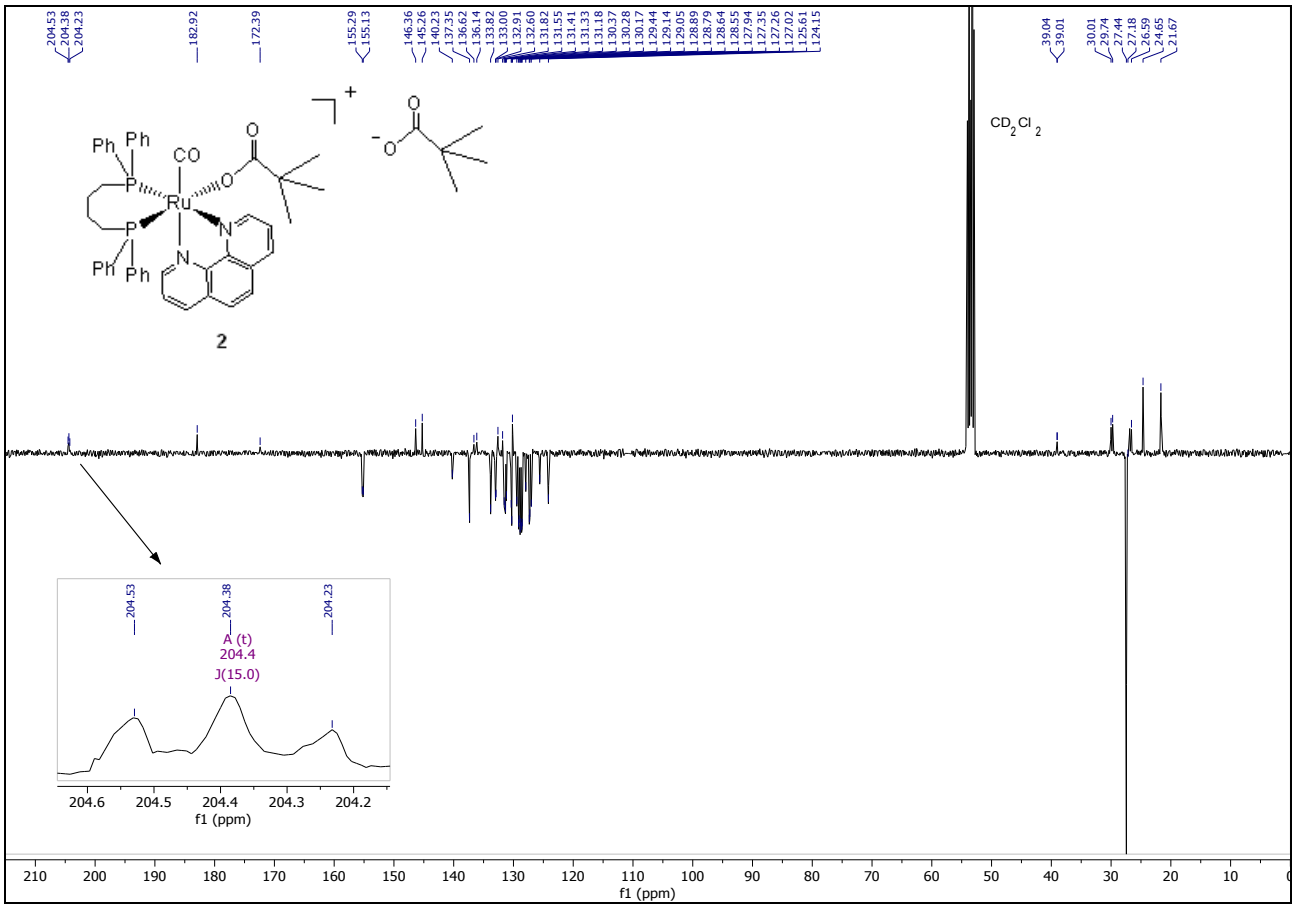

Figure S7. $^{13}C\{^{1}H\}$ DEPTQ NMR spectrum (100.6 MHz) of [Ru(OPiv)(CO)(dppb)(phen)]OPiv (**2**) in CD_2Cl_2 at 298 K.

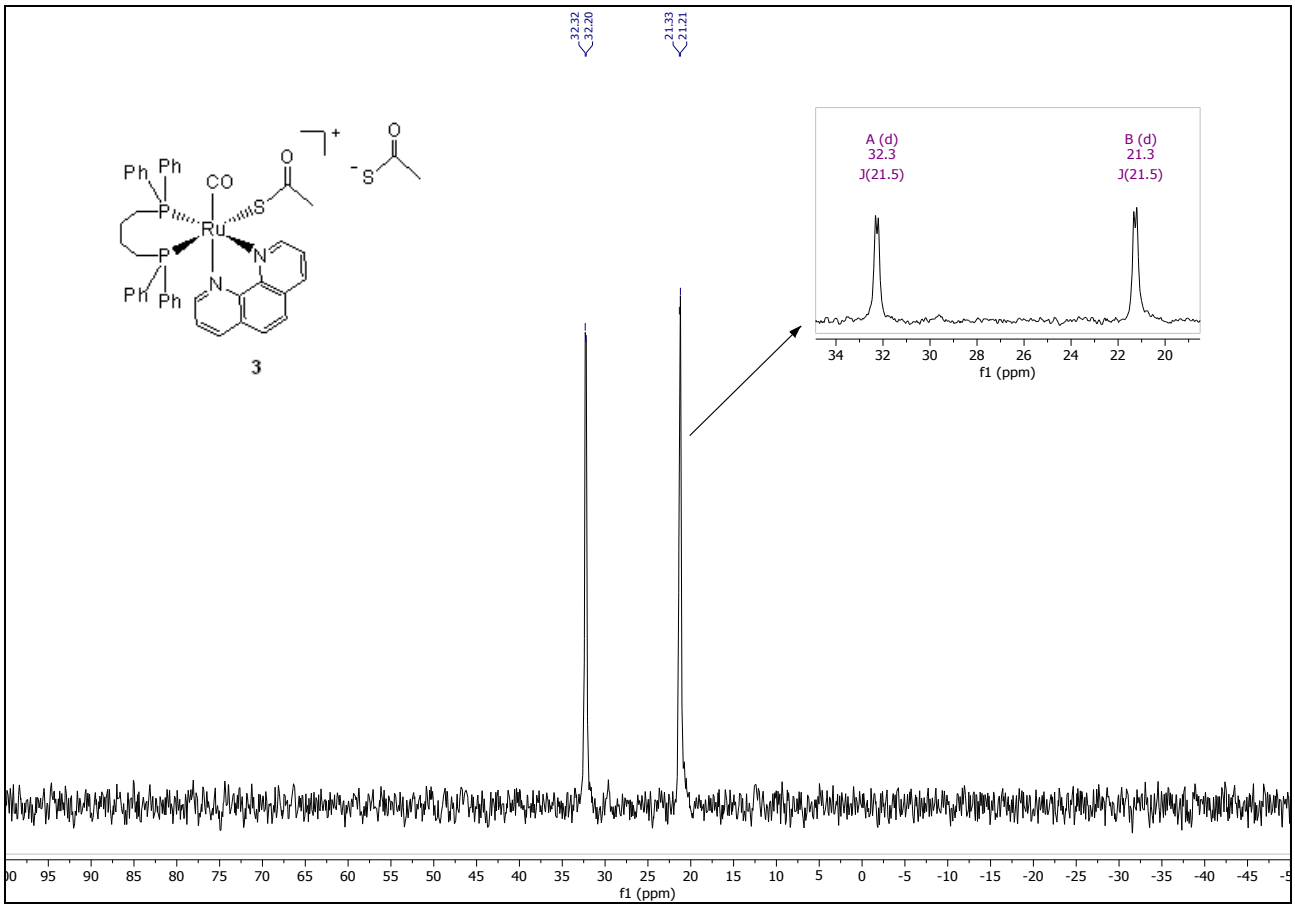

Figure S8. $^{31}P\{^{1}H\}$ NMR spectrum (162 MHz) of [Ru(SAc)(CO)(dppb)(phen)]SAc (**3**) in CD_2Cl_2 at 298 K.

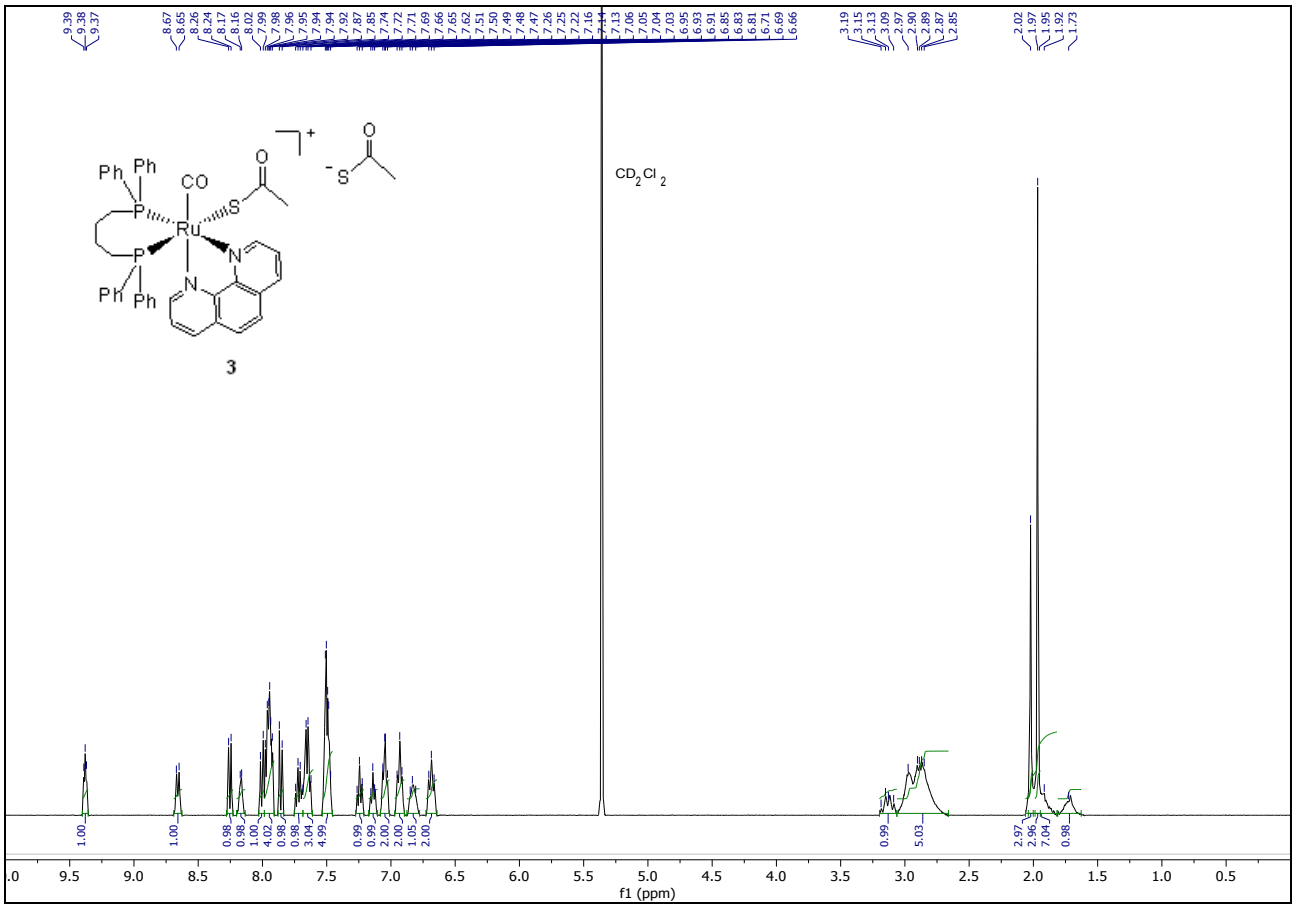

Figure S9. ^{1}H NMR spectrum (400.1 MHz) of [Ru(SAc)(CO)(dppb)(phen)]SAc (**3**) in CD_2Cl_2 at 298 K.

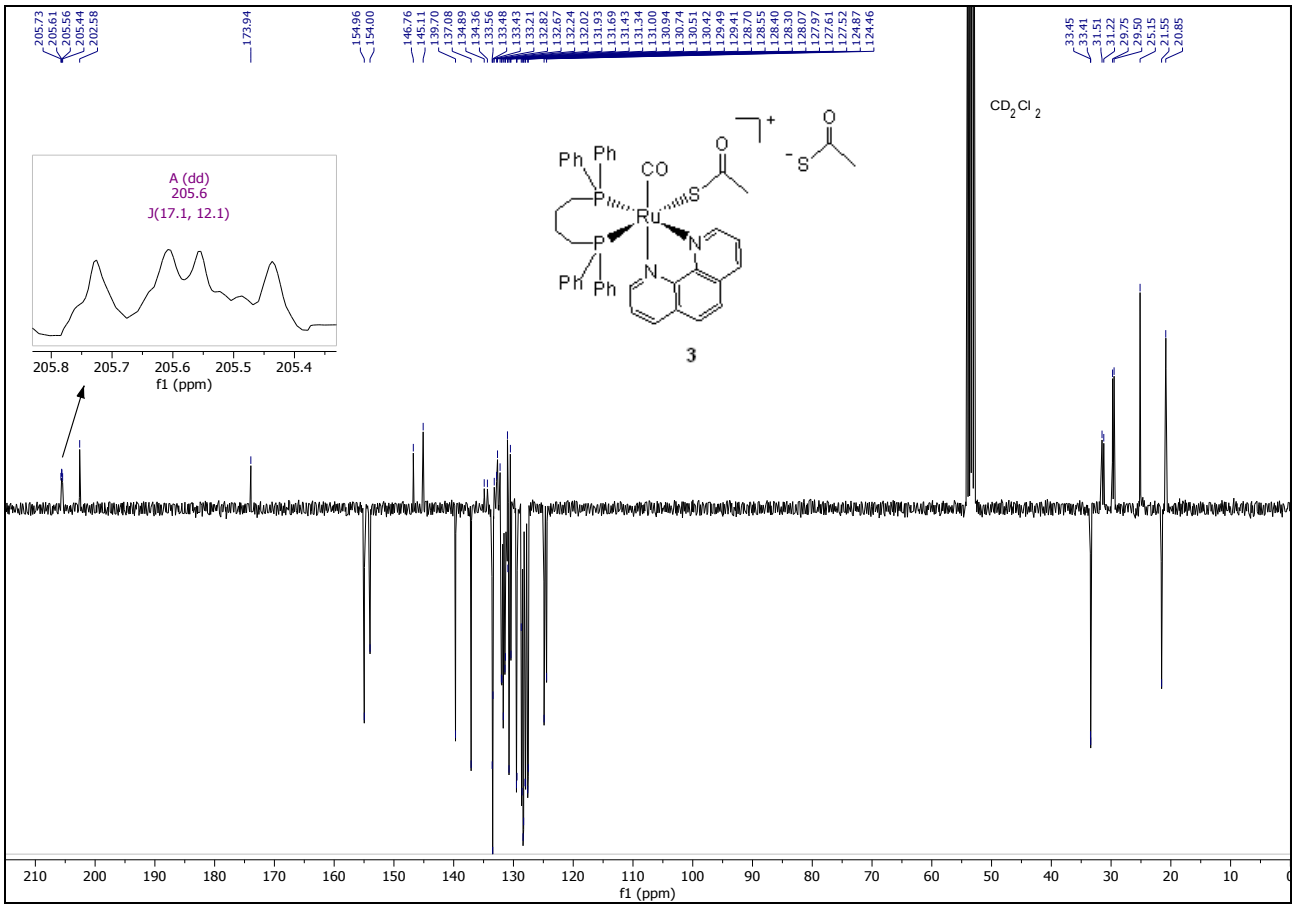

Figure S10. $^{13}C\{^{1}H\}$ DEPTQ NMR spectrum (100.6 MHz) of [Ru(SAc)(CO)(dppb)(phen)]SAc (**3**) in CD_2Cl_2 at 298 K.

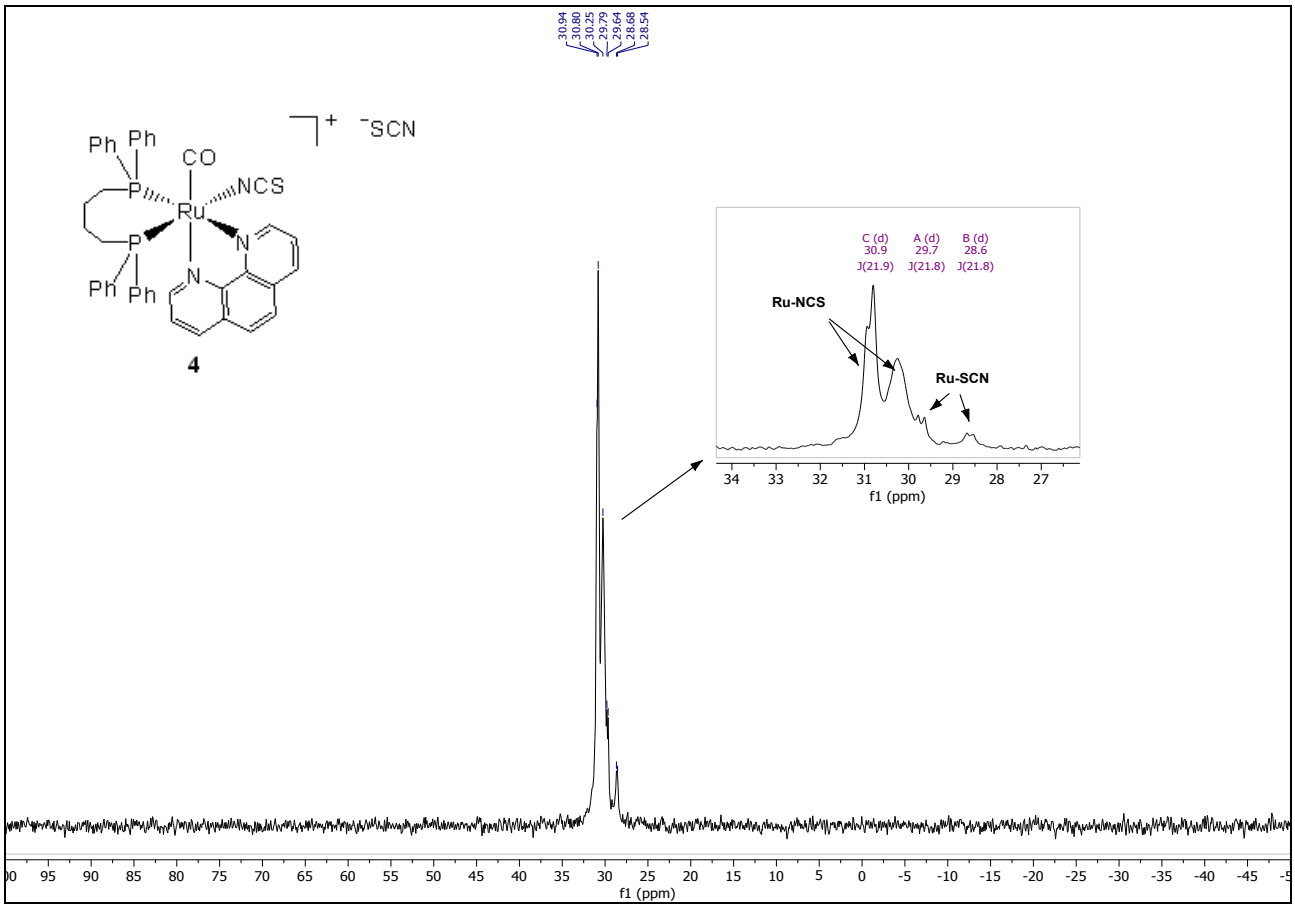

Figure S11. $^{31}P\{^{1}H\}$ NMR spectrum (162 MHz) of [Ru(NCS)(CO)(dppb)(phen)]SCN (**4**) in $CDCl_3$ at 298 K.

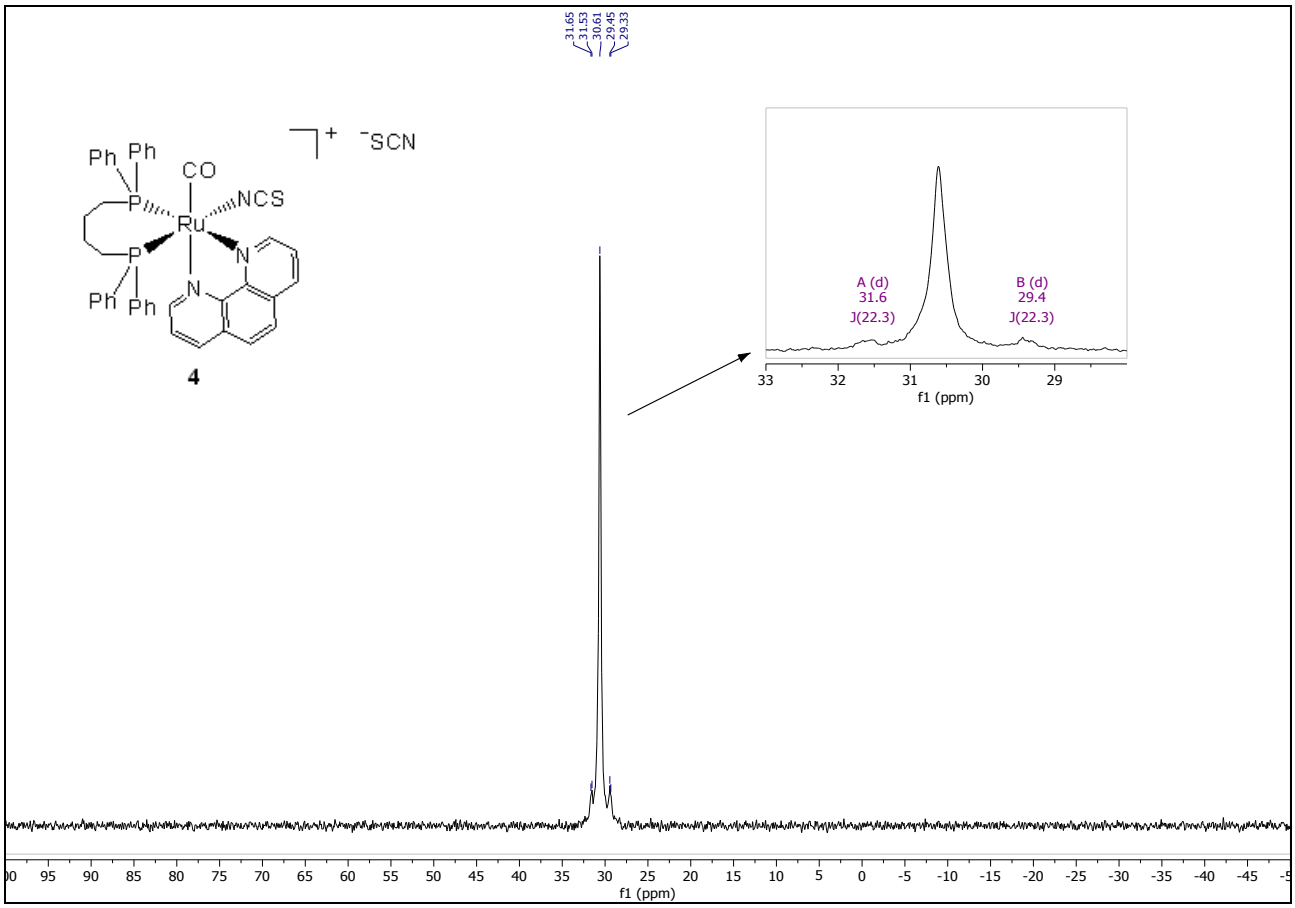

Figure S12. $^{31}P\{^{1}H\}$ NMR spectrum (162 MHz) of [Ru(NCS)(CO)(dppb)(phen)]SCN (**4**) in CD_2Cl_2 at 298 K.

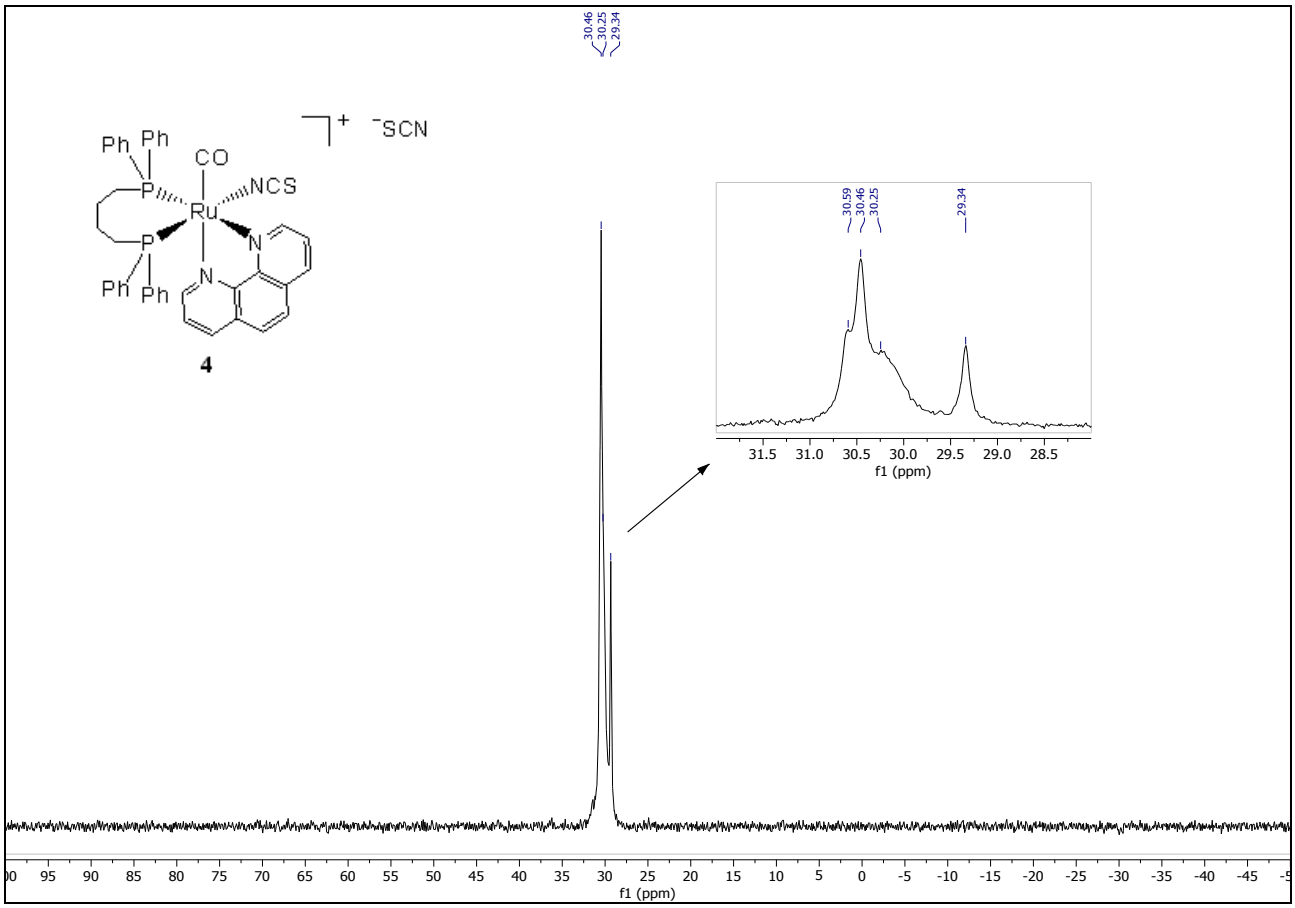

Figure S13. $^{31}P\{^{1}H\}$ NMR spectrum (162 MHz) of [Ru(NCS)(CO)(dppb)(phen)]SCN (**4**) in CD_3OD at 298 K.

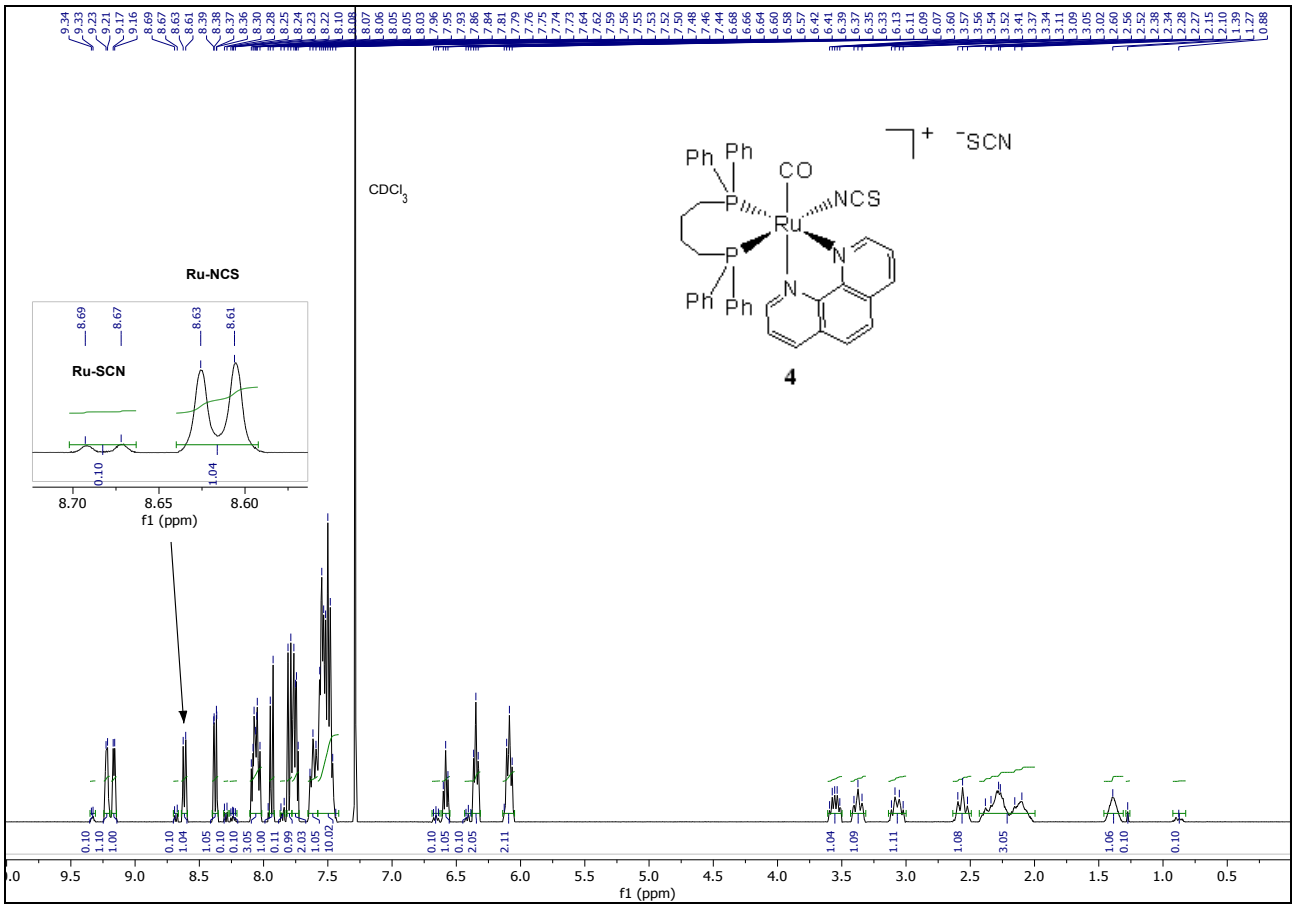

Figure S14. ^{1}H NMR spectrum (400.1 MHz) of [Ru(NCS)(CO)(dppb)(phen)]SCN (**4**) in $CDCl_3$ at 298 K.

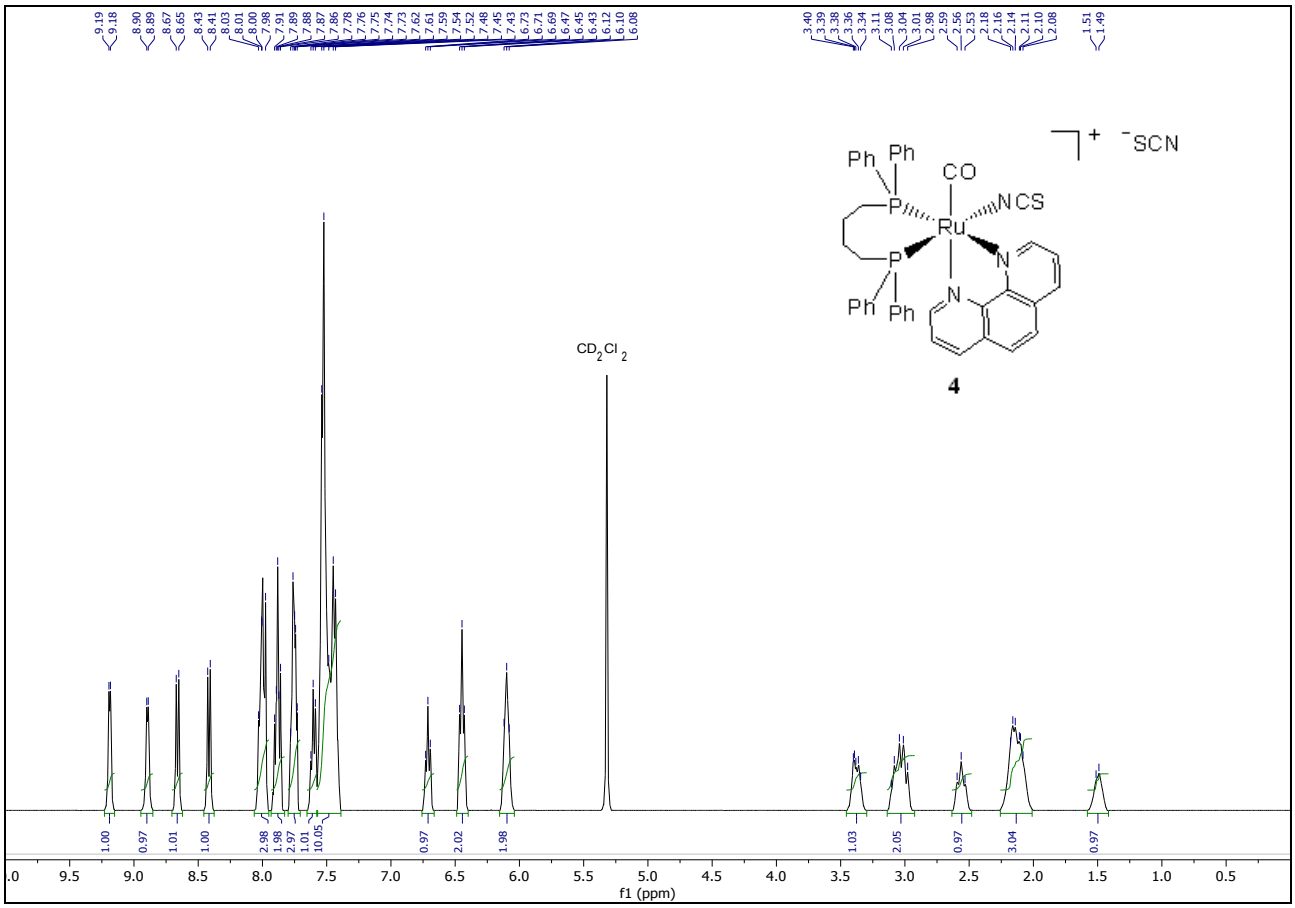

Figure S15. ^{1}H NMR spectrum (400.1 MHz) of [Ru(NCS)(CO)(dppb)(phen)]SCN (**4**) in CD_2Cl_2 at 298 K.

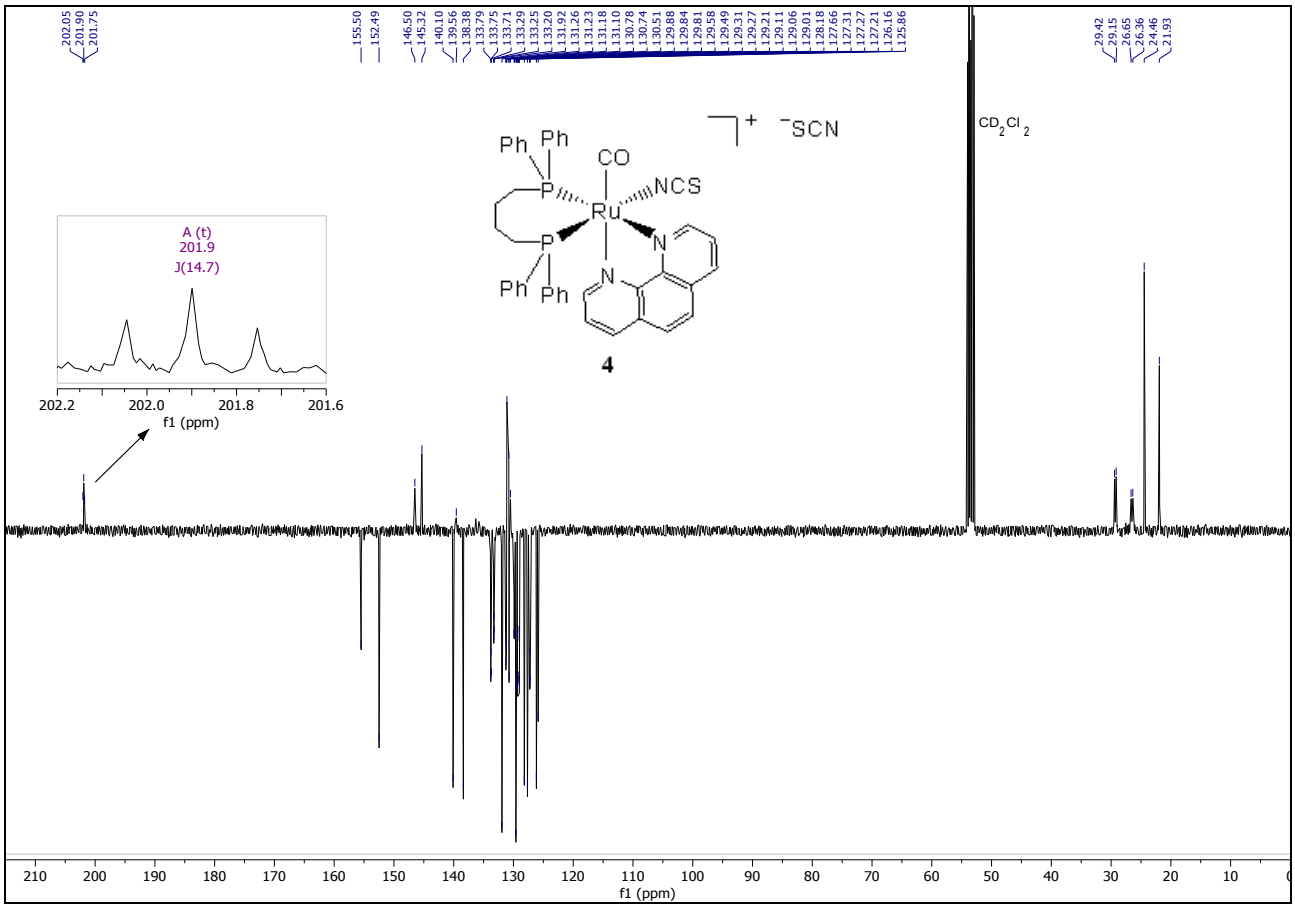

Figure S16. $^{13}C\{^{1}H\}$ DEPTQ NMR spectrum (100.6 MHz) of [Ru(NCS)(CO)(dppb)(phen)]SCN (**4**) in CD_2Cl_2 at 298 K.

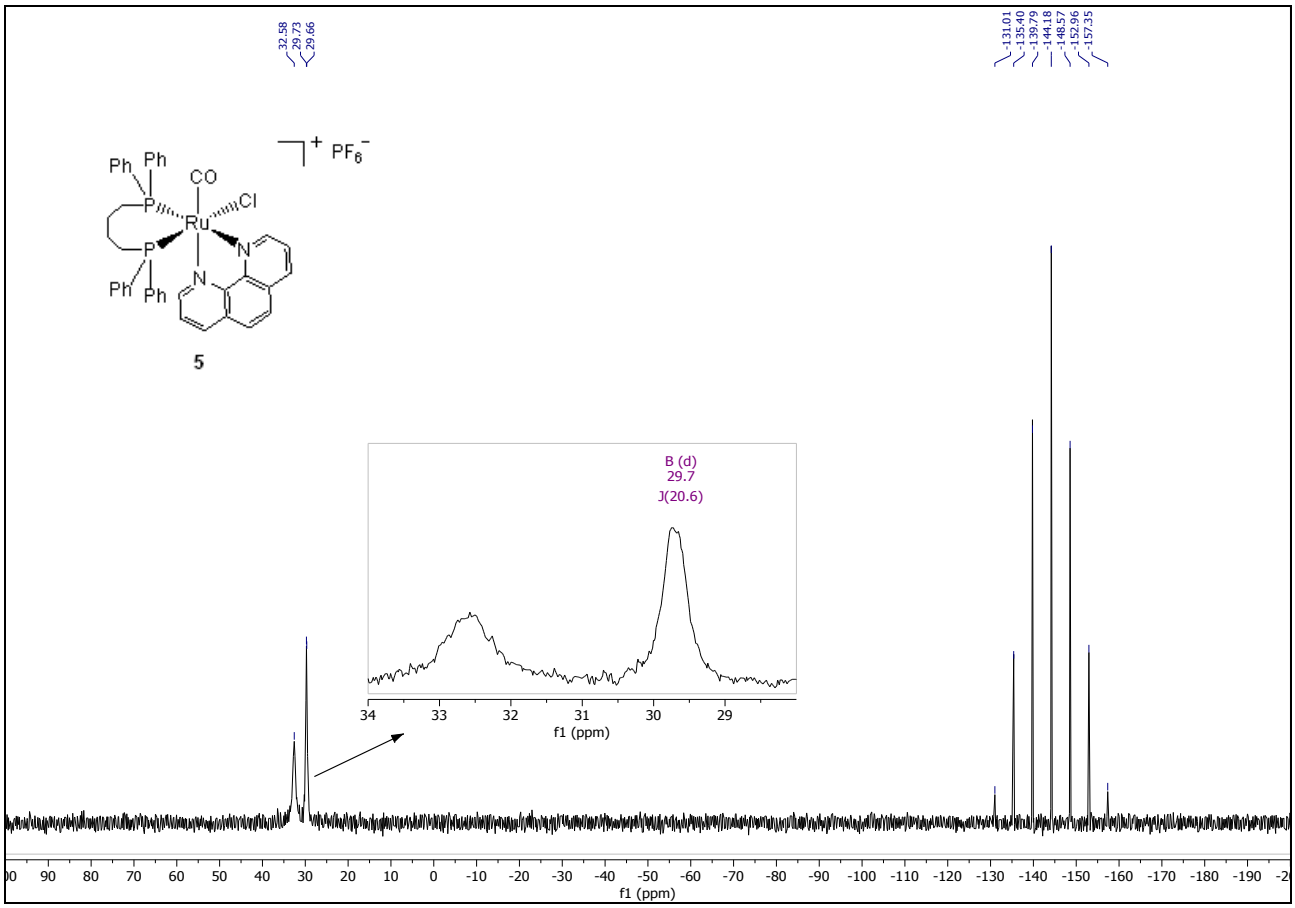

Figure S17. $^{31}P\{^{1}H\}$ NMR spectrum (162 MHz) of [Ru(Cl)(CO)(dppb)(phen)]PF_6 (**5**) in DMSO-d_6 at 298 K.

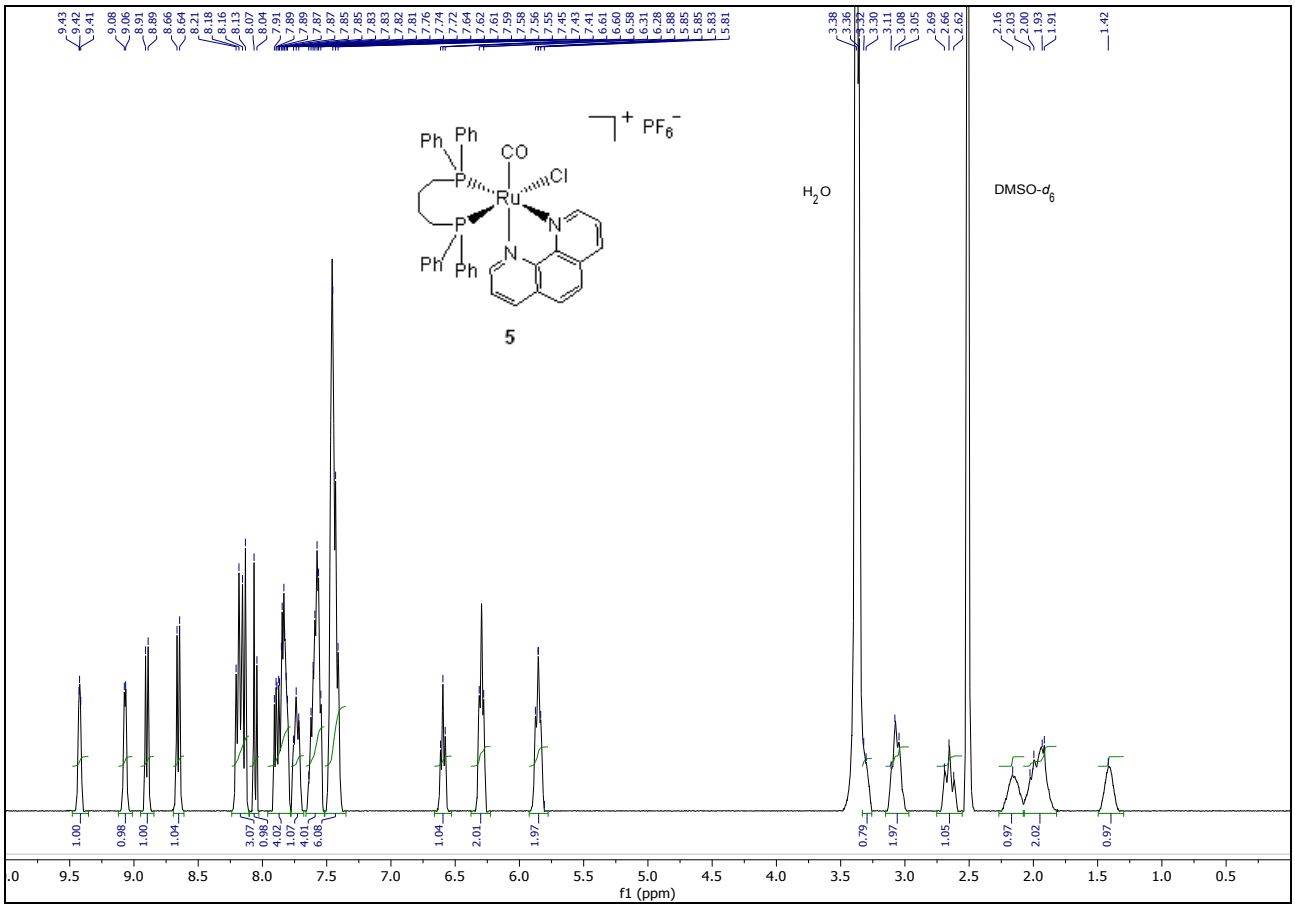

Figure S18. ^{1}H NMR spectrum (400.1 MHz) of [Ru(Cl)(CO)(dppb)(phen)]PF_6 (**5**) in DMSO-d_6 at 298 K.

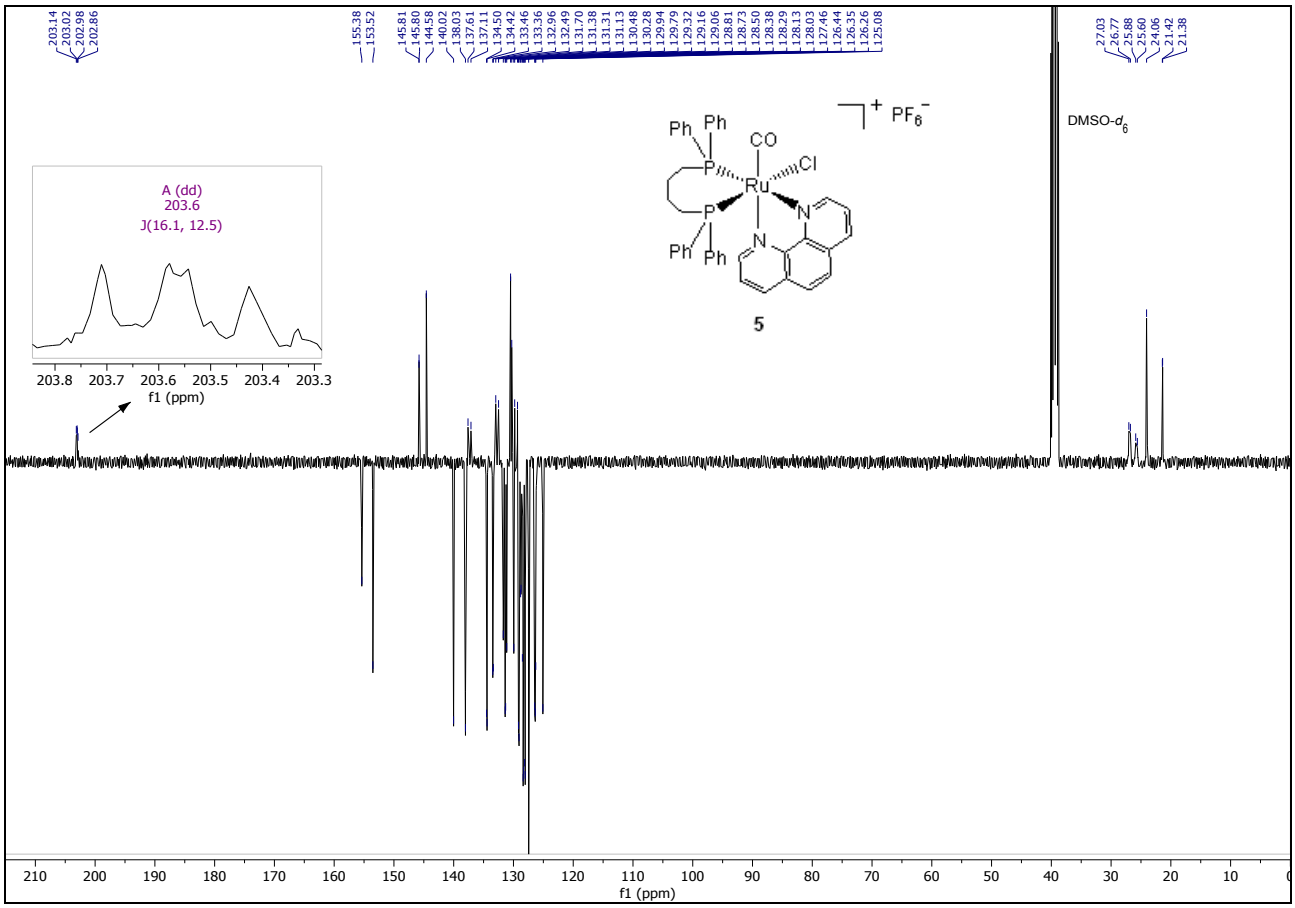

Figure S19. $^{13}C\{^{1}H\}$ DEPTQ NMR spectrum (100.6 MHz) of [Ru(Cl)(CO)(dppb)(phen)]PF_6 (**5**) in DMSO-d_6 at 298 K.

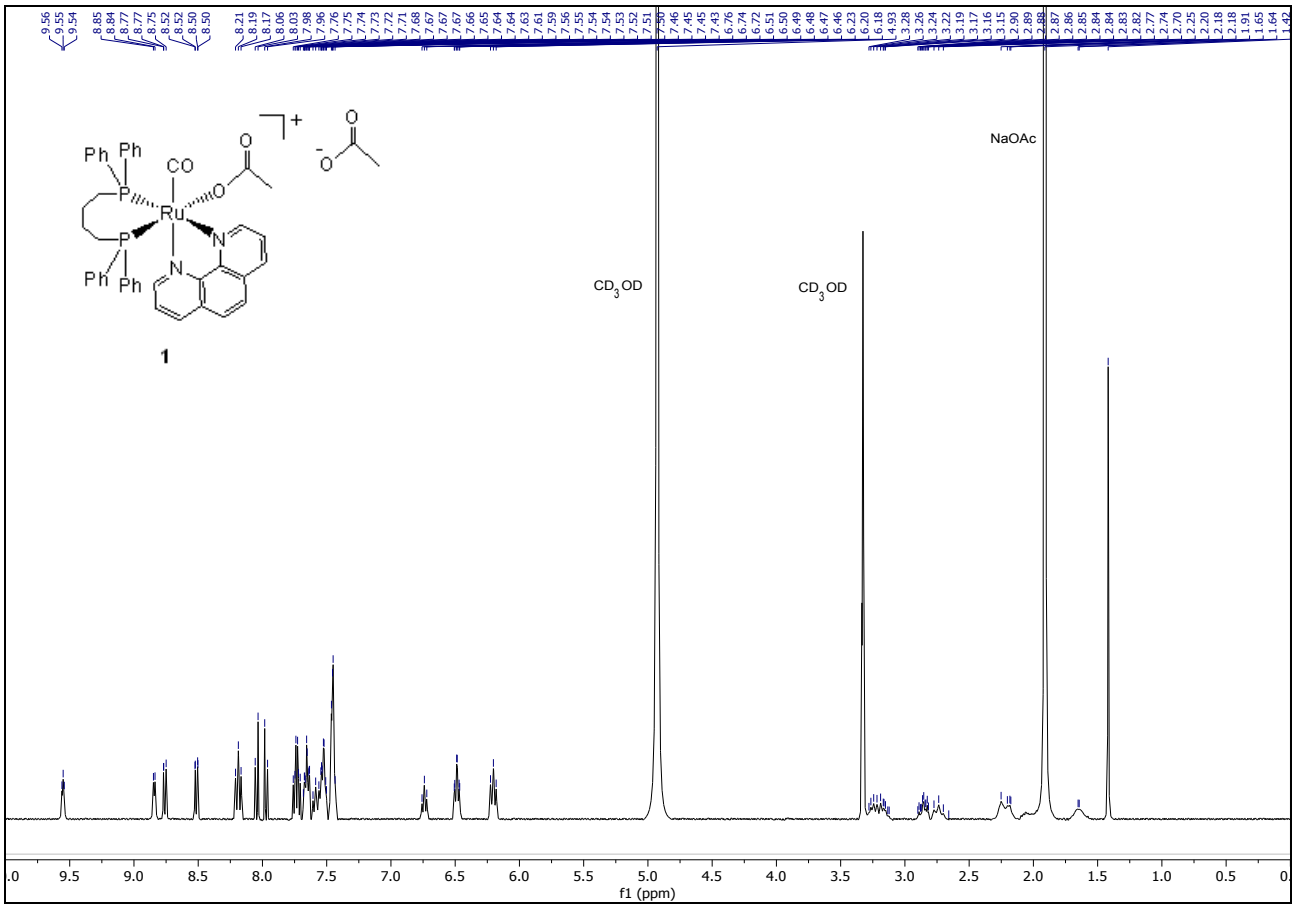

Figure S20. Effect of the addition of NaOAc (15 equiv) to [Ru(OAc)(CO)(dppb)(phen)]OAc (**1**) in the ^{1}H NMR spectrum (400.1 MHz) in CD_3OD at 298 K.

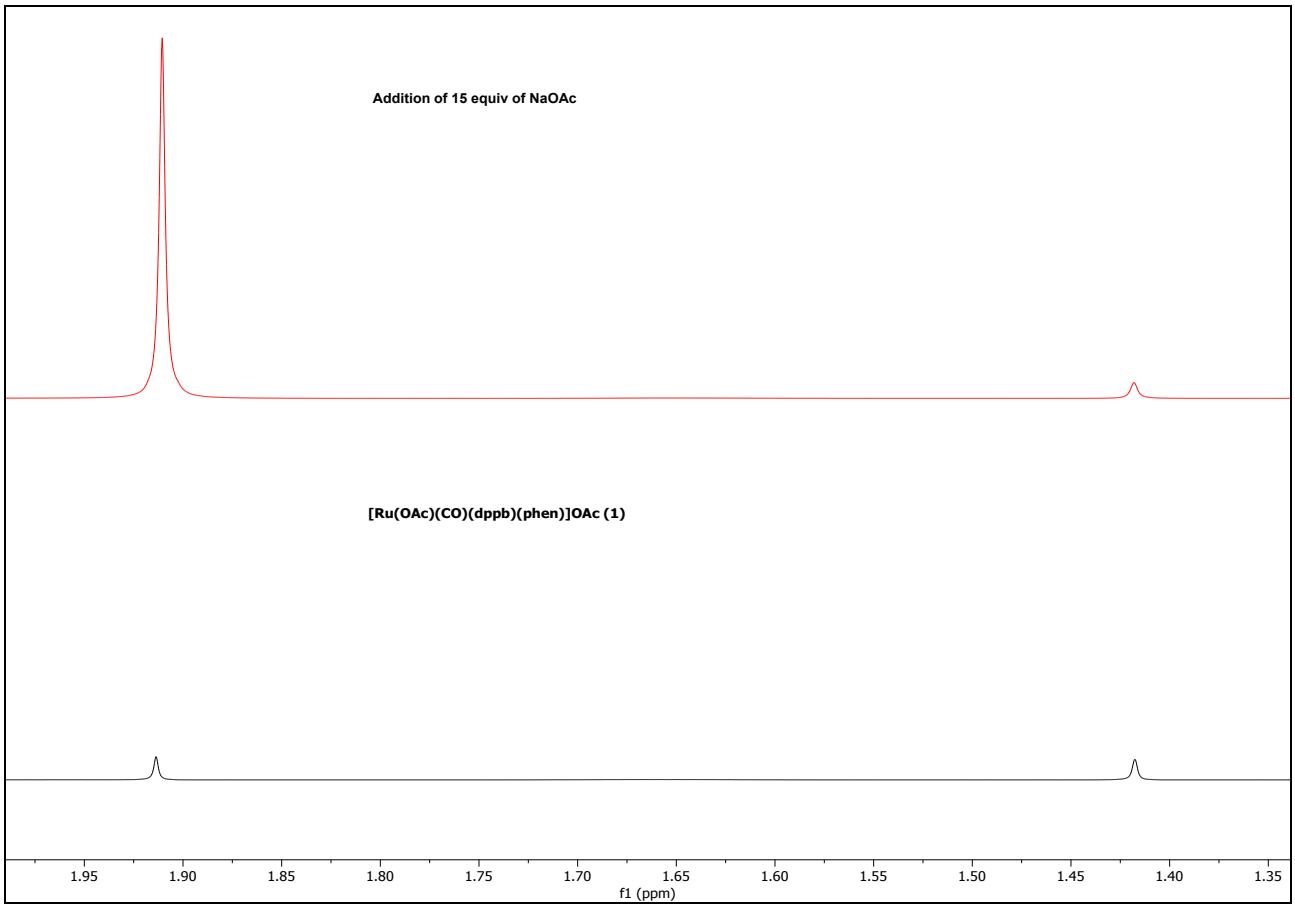

Figure S21. Effect of the addition of NaOAc (15 equiv) to [Ru(OAc)(CO)(dppb)(phen)]OAc (**1**) in the methyl acetate region of the ^{1}H NMR spectra (400.1 MHz) in CD_3OD at 298 K.

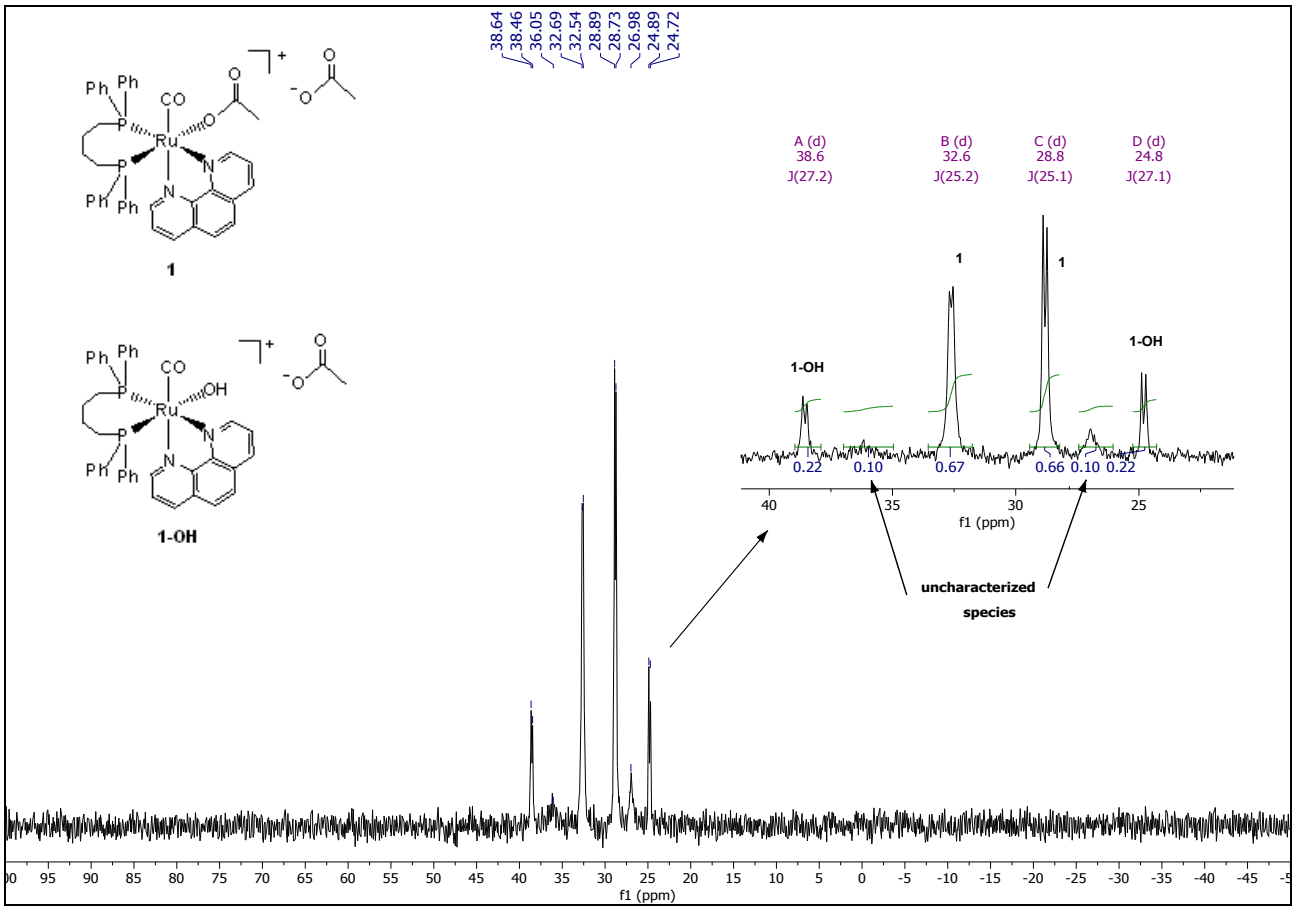

Figure S22. $^{31}P\{^{1}H\}$ NMR spectrum (162 MHz) of [Ru(OAc)(CO)(dppb)(phen)]OAc (**1**) in D_2O at 298 K.

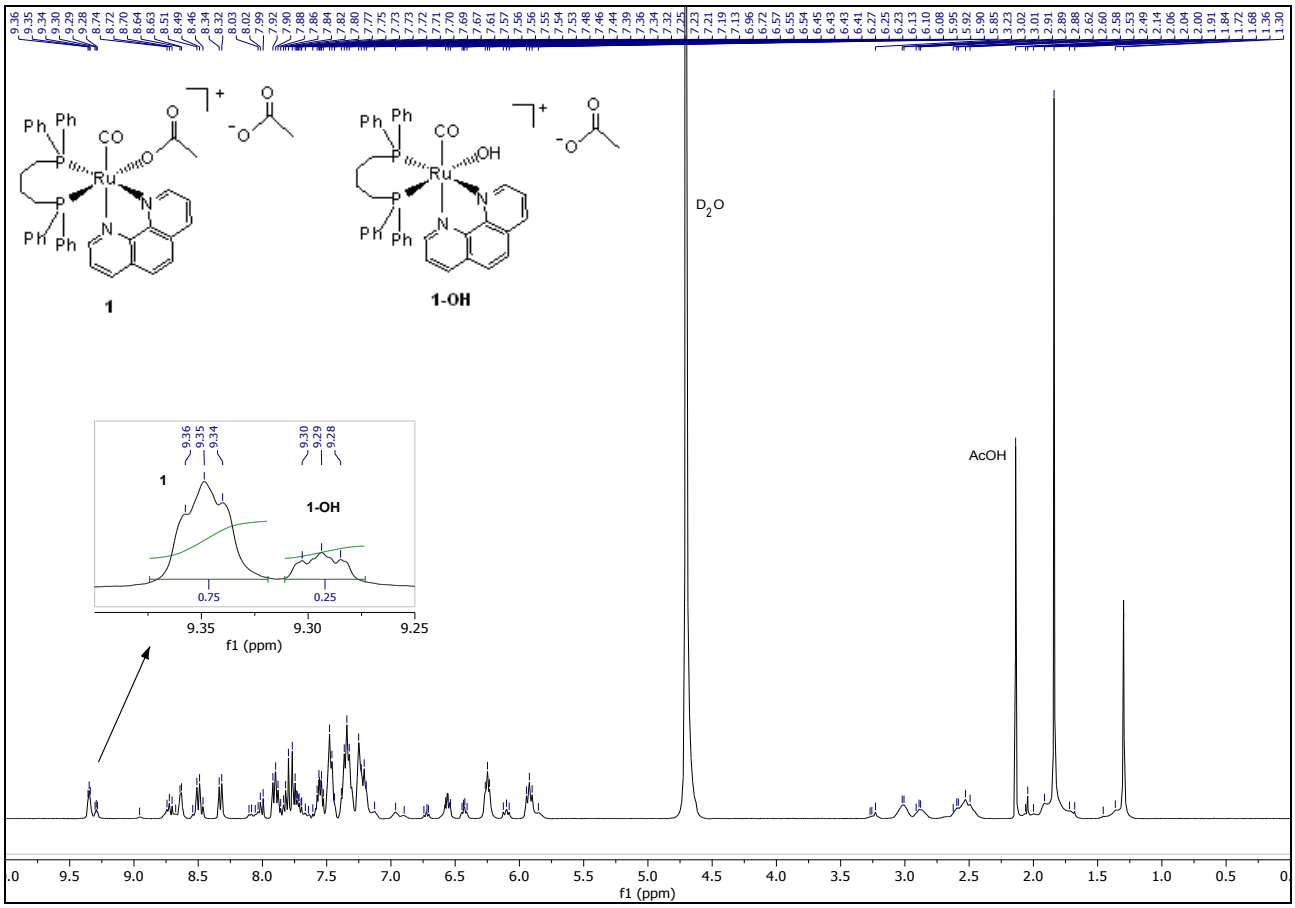

Figure S23. ^{1}H NMR spectrum (400.1 MHz) of [Ru(OAc)(CO)(dppb)(phen)]OAc (**1**) in D_2O at 298 K.

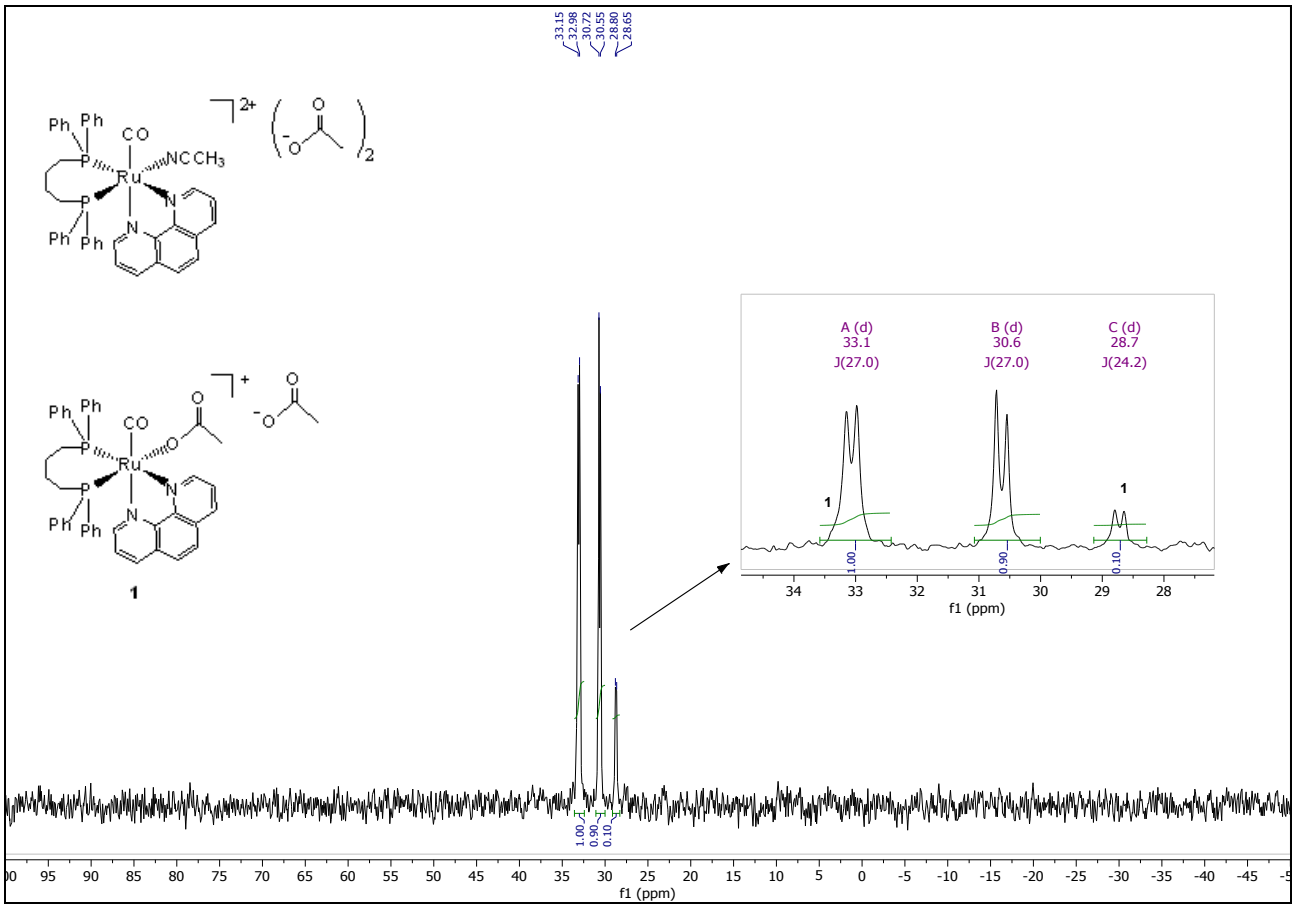

Figure S24. $^{31}P\{^{1}H\}$ NMR spectrum (162 MHz) of the products of the reaction between [Ru(OAc)(CO)(dppb)(phen)]OAc (**1**) and CH_3CN (10 equiv) in D_2O at 298 K.

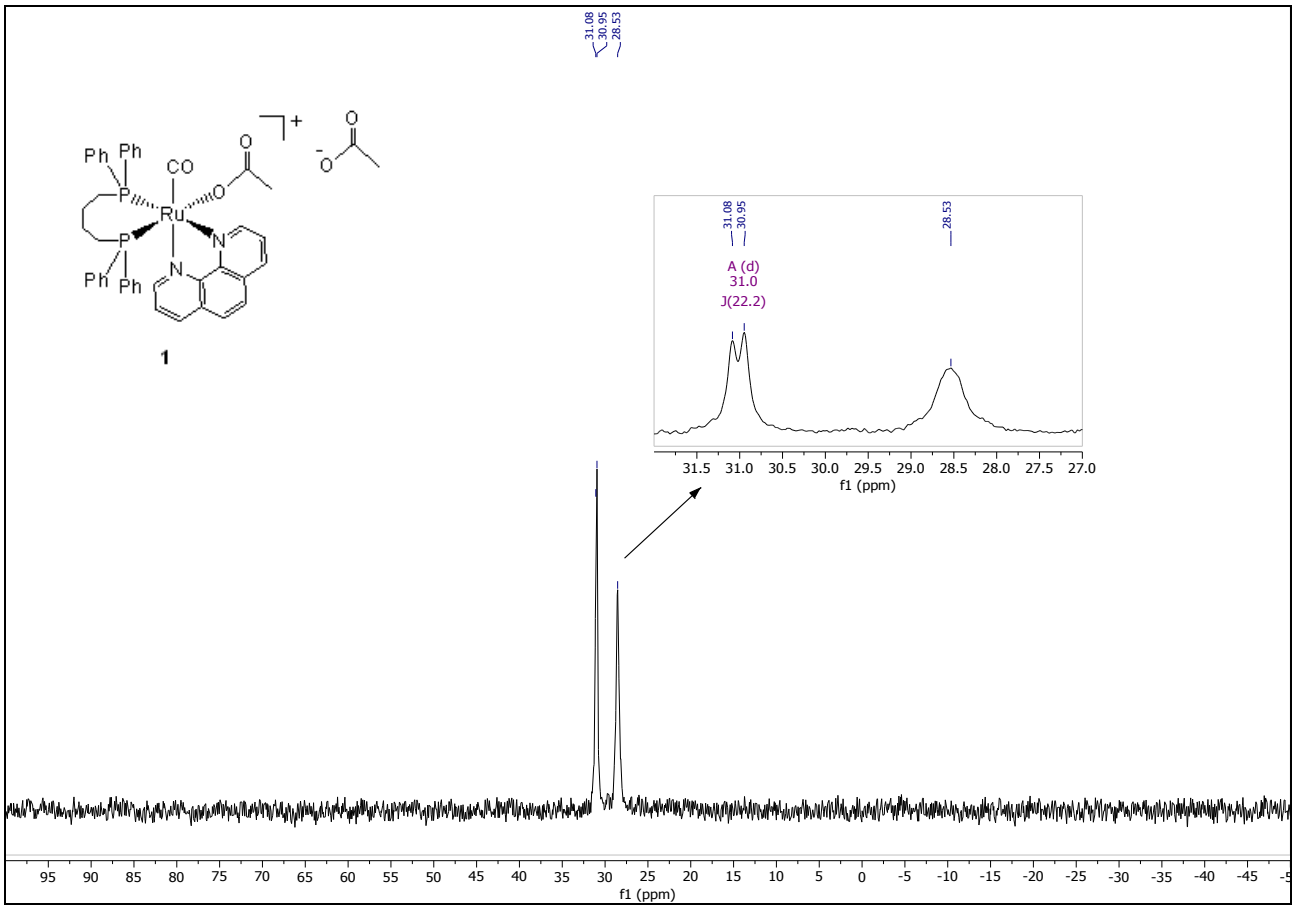

Figure S25. $^{31}P\{^{1}H\}$ NMR spectrum (162 MHz) of [Ru(OAc)(CO)(dppb)(phen)]OAc (**1**) in DMSO-d_6 at 298 K after 48 h.

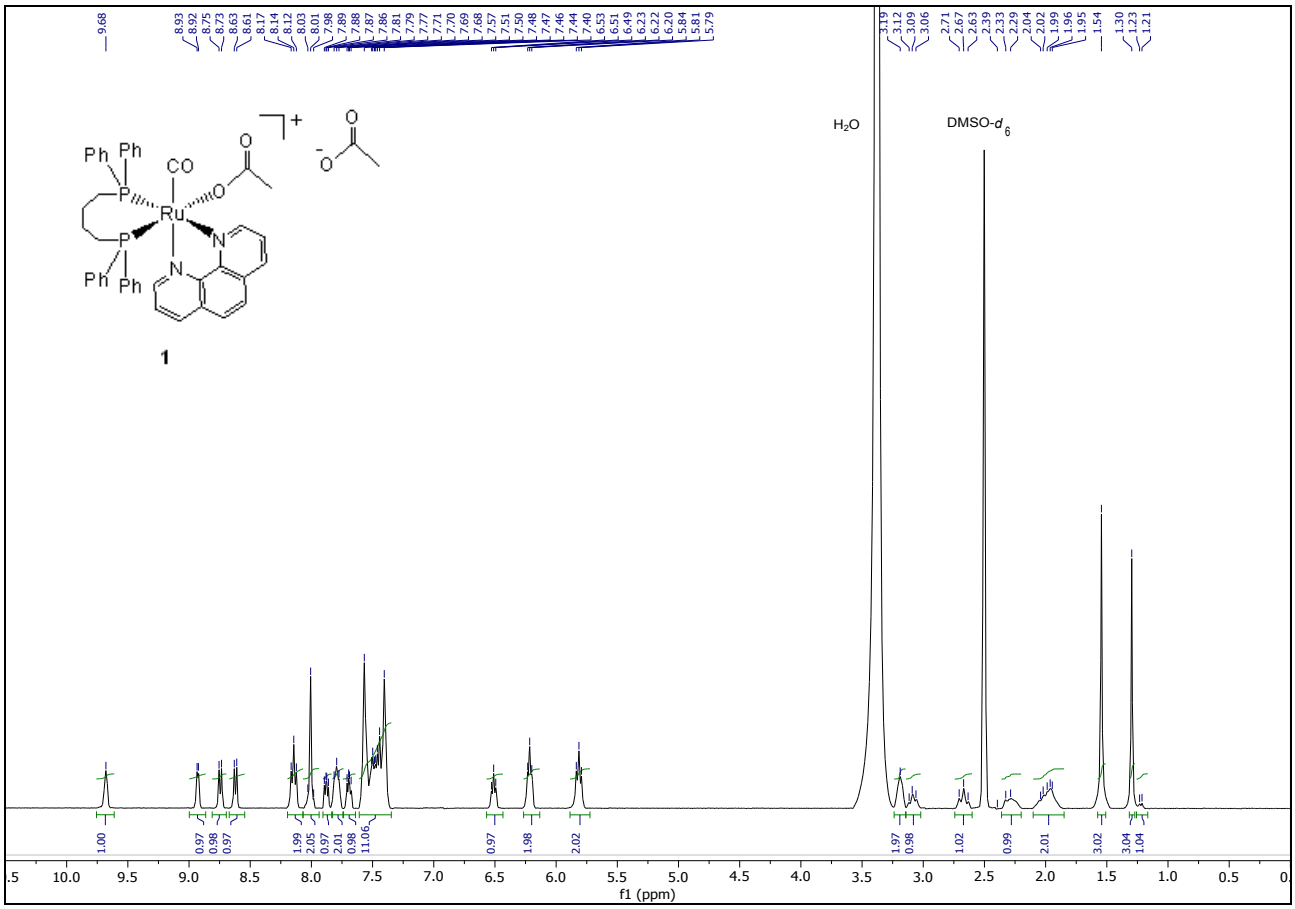

Figure S26. ^{1}H NMR spectrum (400.1 MHz) of [Ru(OAc)(CO)(dppb)(phen)]OAc (**1**) in DMSO-d_6 at 298 K after 48 h.

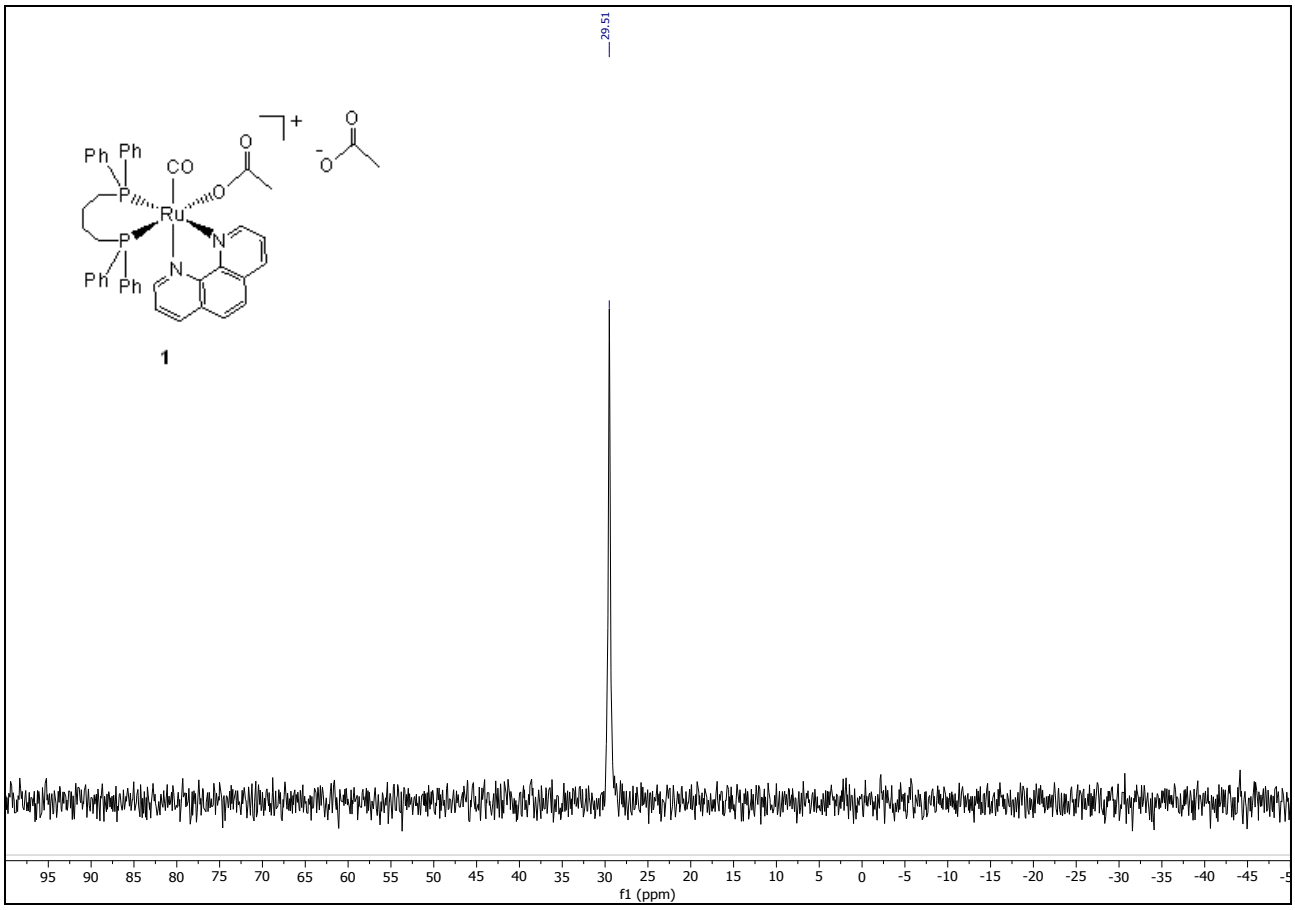

Figure S27. $^{31}P\{^{1}H\}$ NMR spectrum (162 MHz) of [Ru(OAc)(CO)(dppb)(phen)]OAc (**1**) in a DMSO-d_6/D_2O mixture (1:1 (v/v)) at 298 K after 24 h.

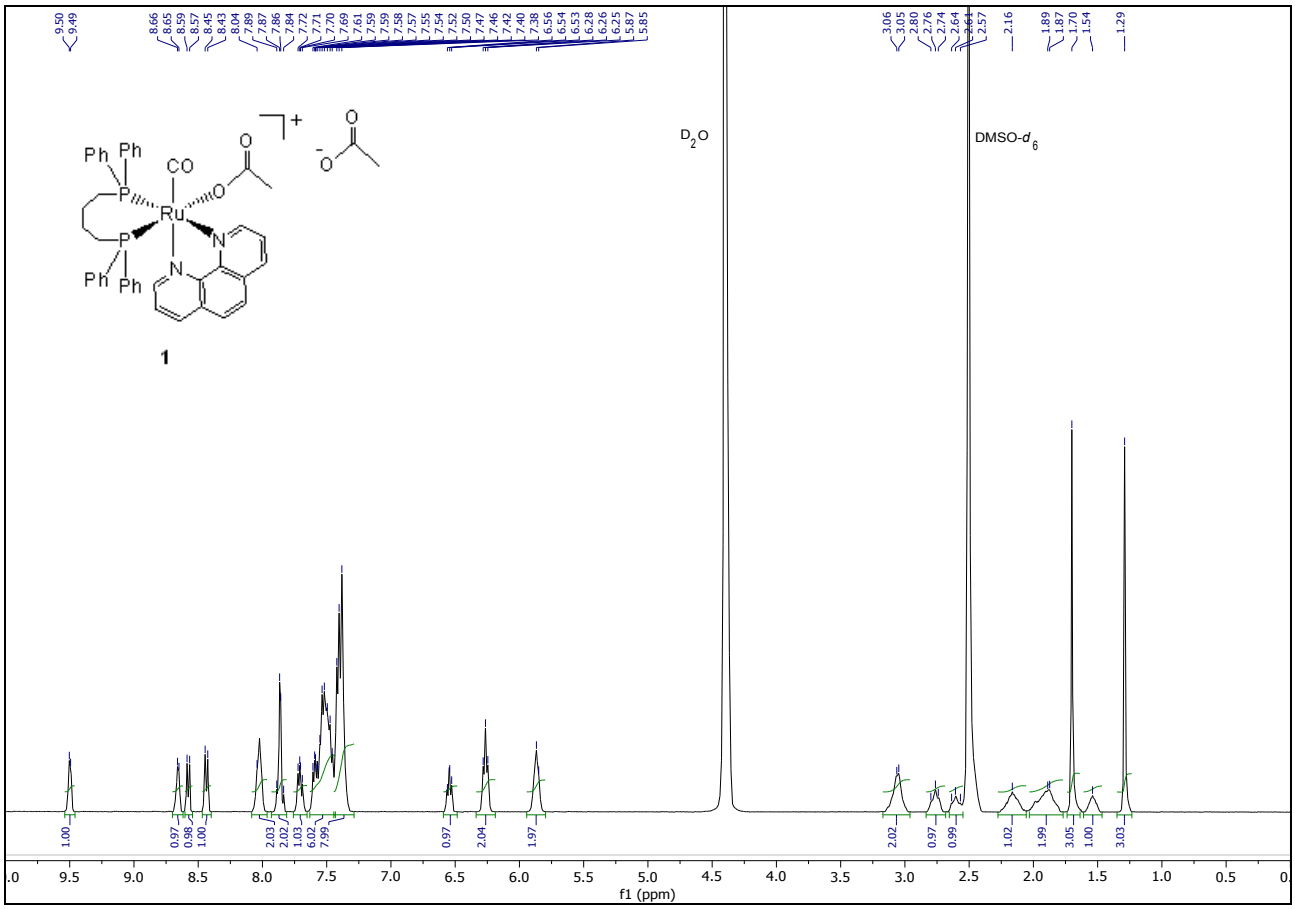

Figure S28. ^{1}H NMR spectrum (400.1 MHz) of [Ru(OAc)(CO)(dppb)(phen)]OAc (**1**) in a DMSO-d_6/D_2O mixture (1:1 (v/v)) at 298 K after 24 h.

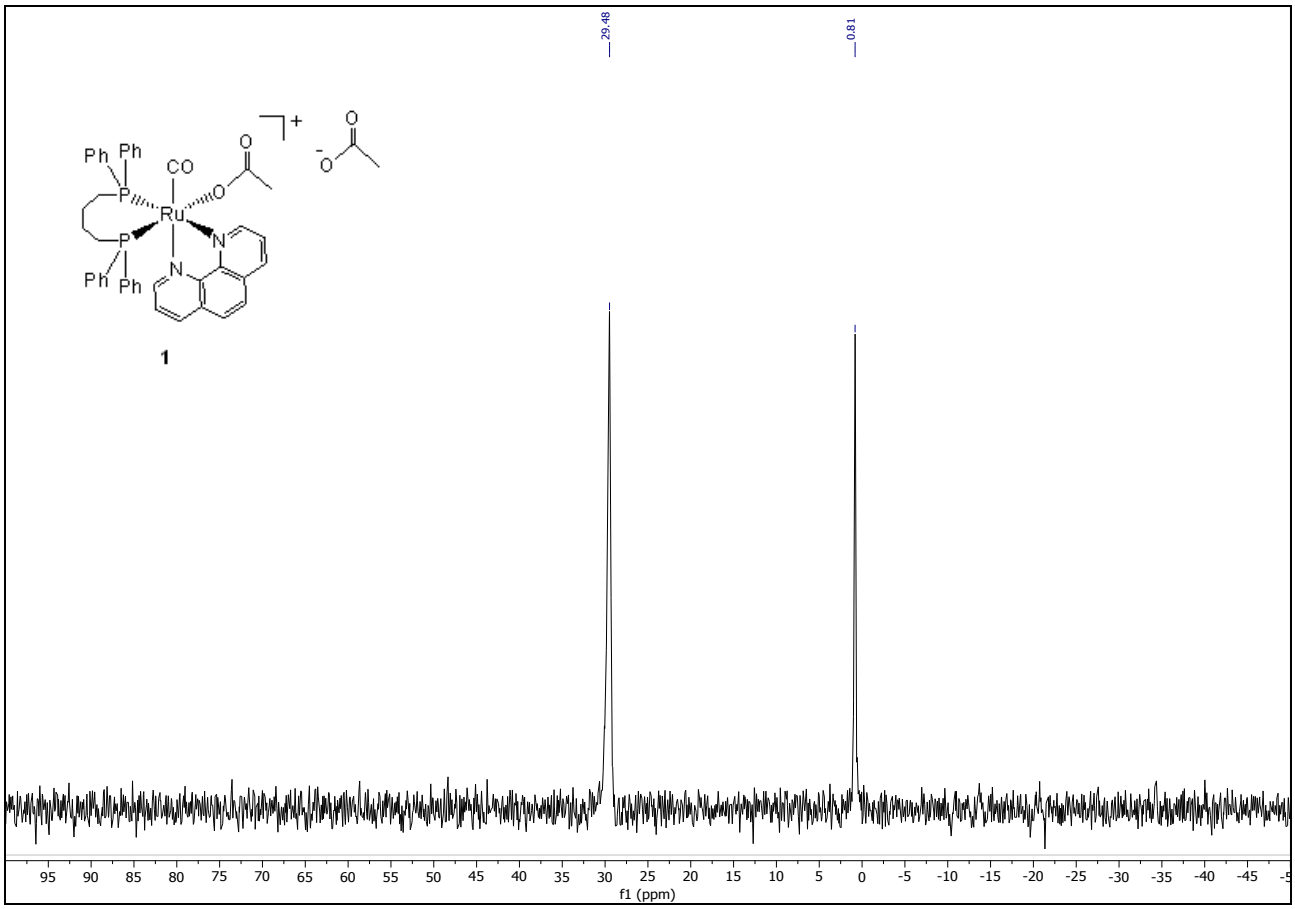

Figure S29. $^{31}P\{^{1}H\}$ NMR spectrum (162 MHz) of [Ru(OAc)(CO)(dppb)(phen)]OAc (**1**) in a DMSO-d_6/RPMI 1640 medium mixture (1:1 (v/v)) at 298 K after 24 h.

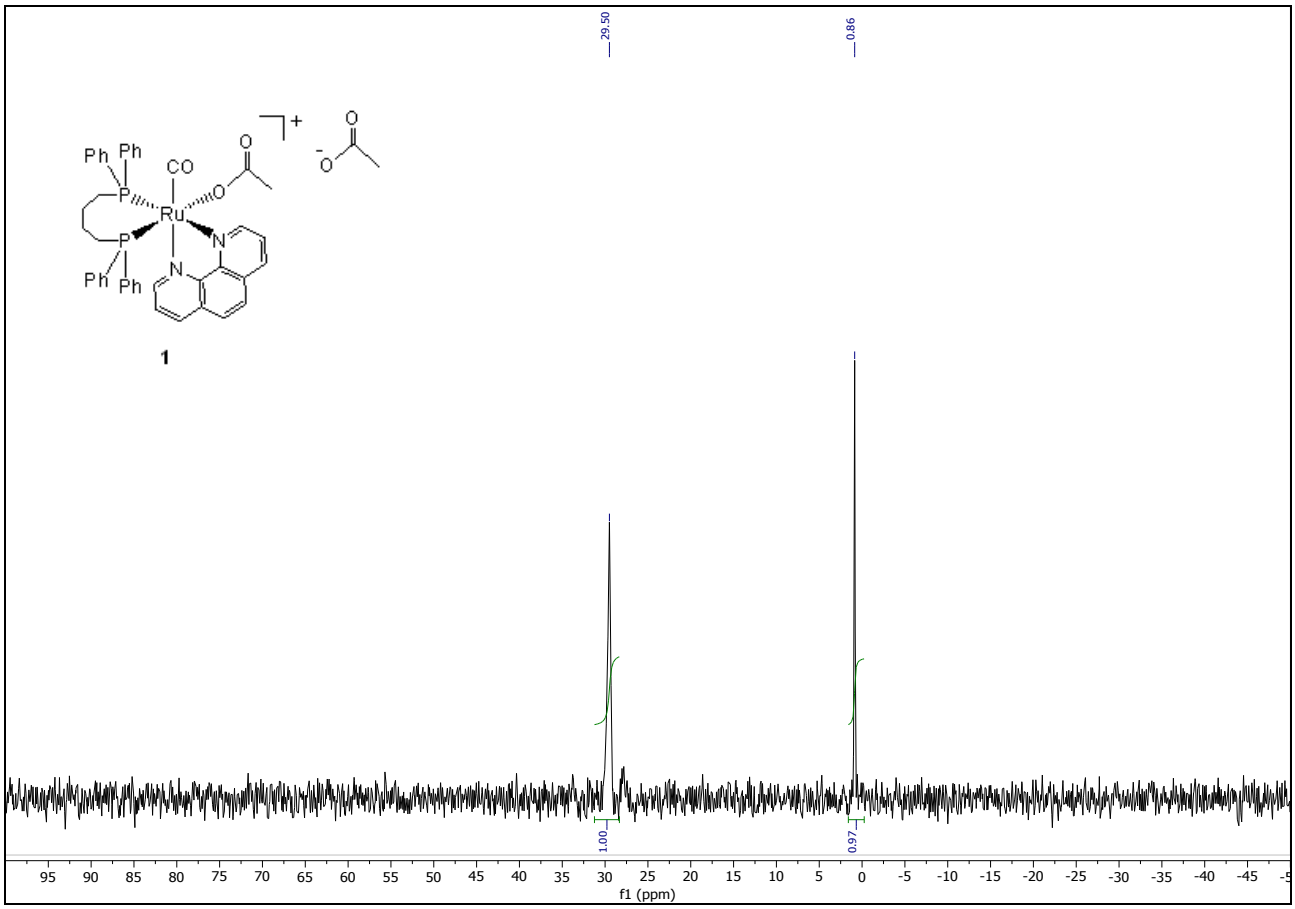

Figure S30. $^{31}P\{^{1}H\}$ NMR spectrum (162 MHz) of [Ru(OAc)(CO)(dppb)(phen)]OAc (**1**) in a DMSO-d_6/RPMI 1640 medium mixture (1:1(v/v)) at 298 K after 48 h.

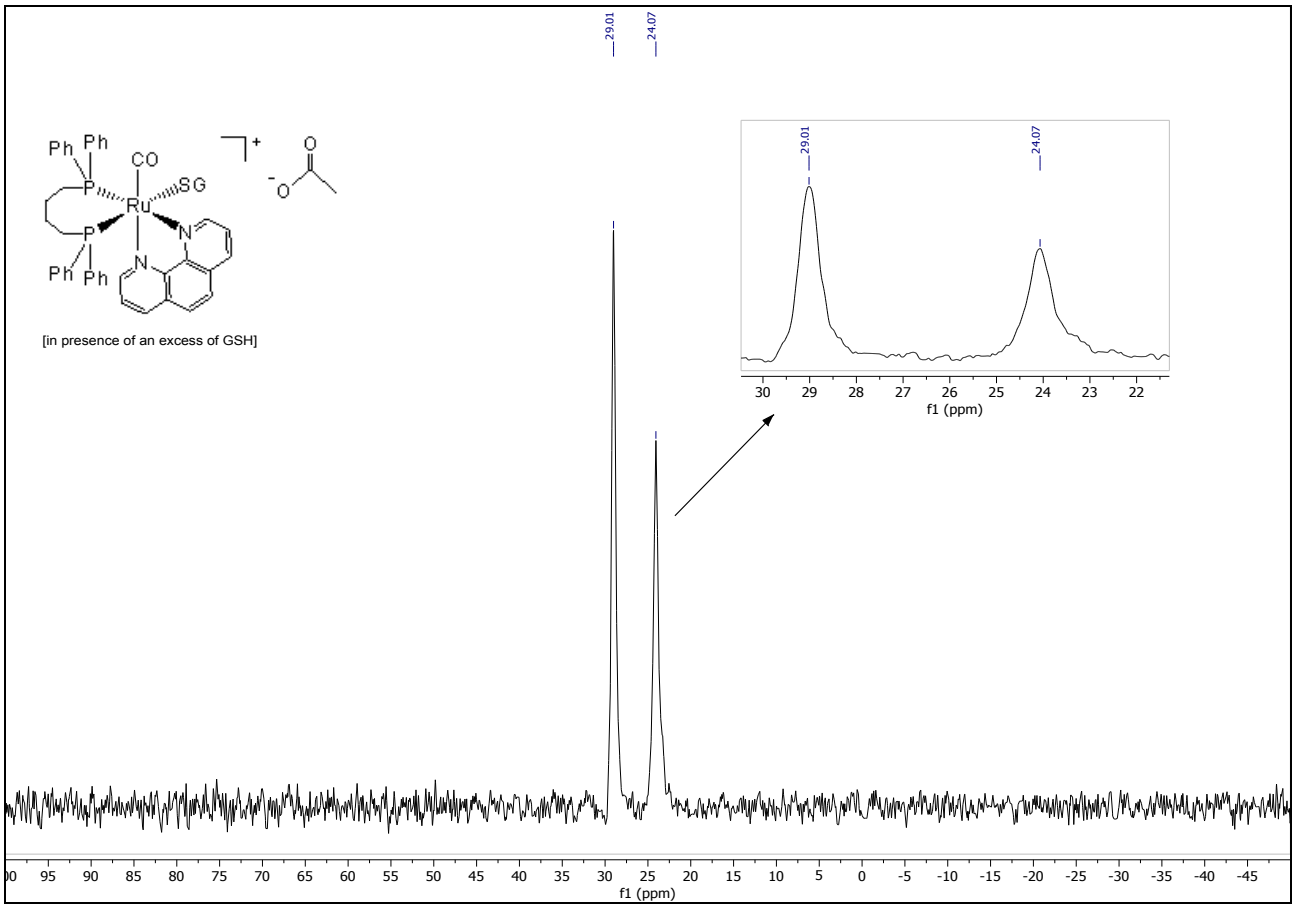

Figure S31. $^{31}P\{^{1}H\}$ NMR spectrum (162 MHz) of the products of the reaction between [Ru(OAc)(CO)(dppb)(phen)]OAc (**1**) and GSH (2 equiv) in D_2O at 298 K.

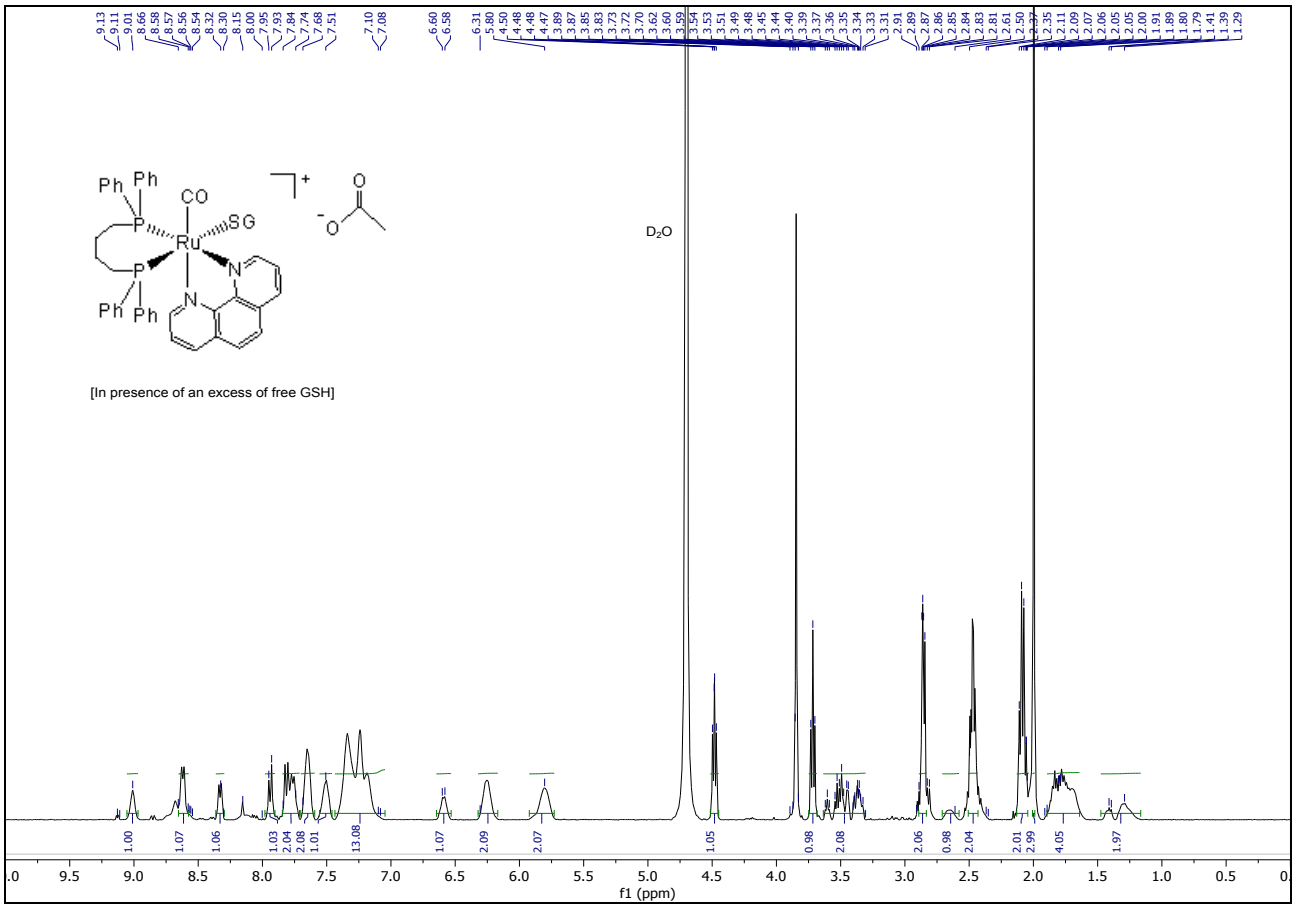

Figure S32. ^{1}H NMR spectrum (400.1 MHz) of the products of the reaction between [Ru(OAc)(CO)(dppb)(phen)]OAc (**1**) and GSH (2 equiv) in D_2O at 298 K.

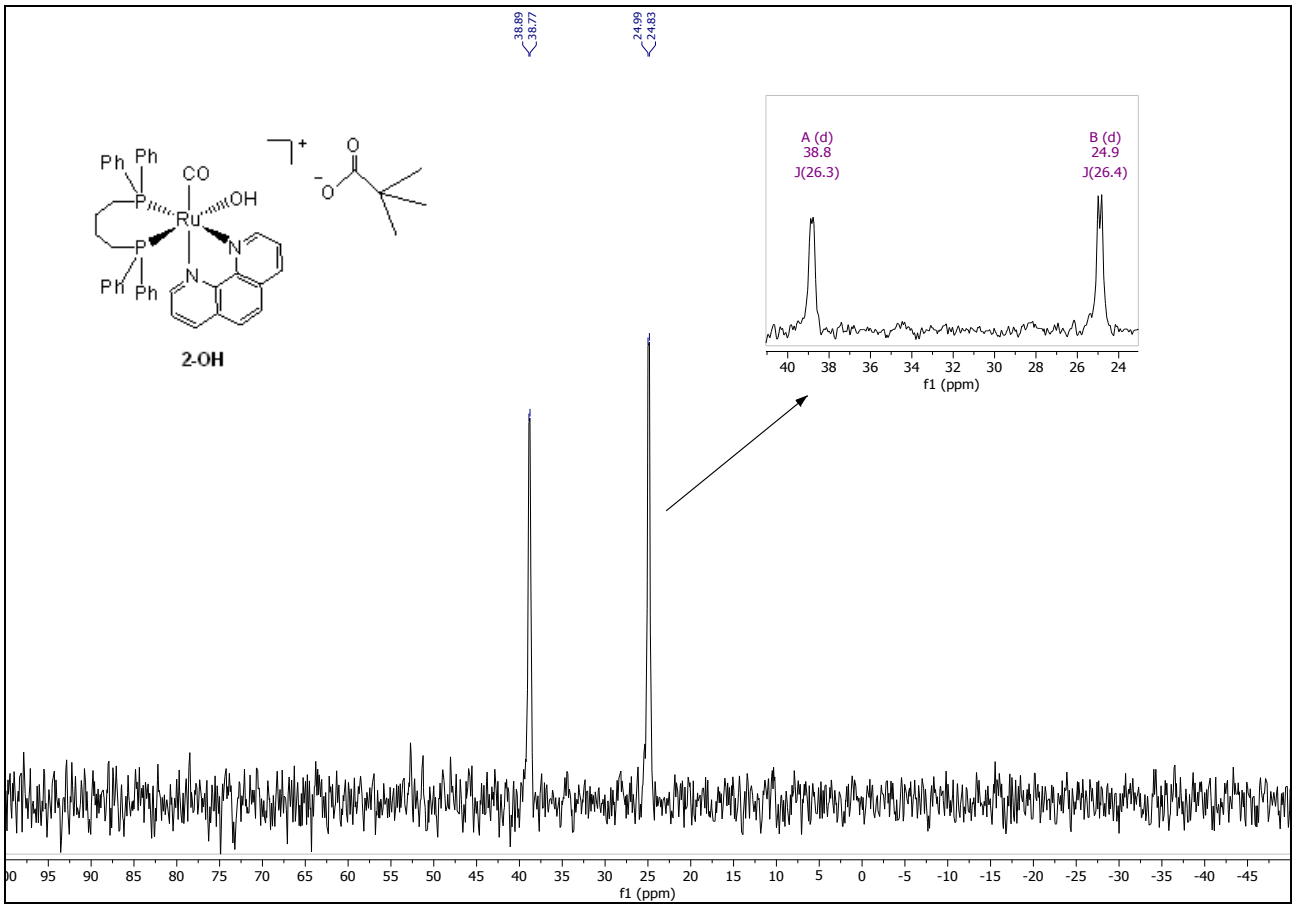

Figure S33. $^{31}P\{^{1}H\}$ NMR spectrum (162 MHz) of [Ru(OPiv)(CO)(dppb)(phen)]OPiv (**2**) in D_2O at 298 K.

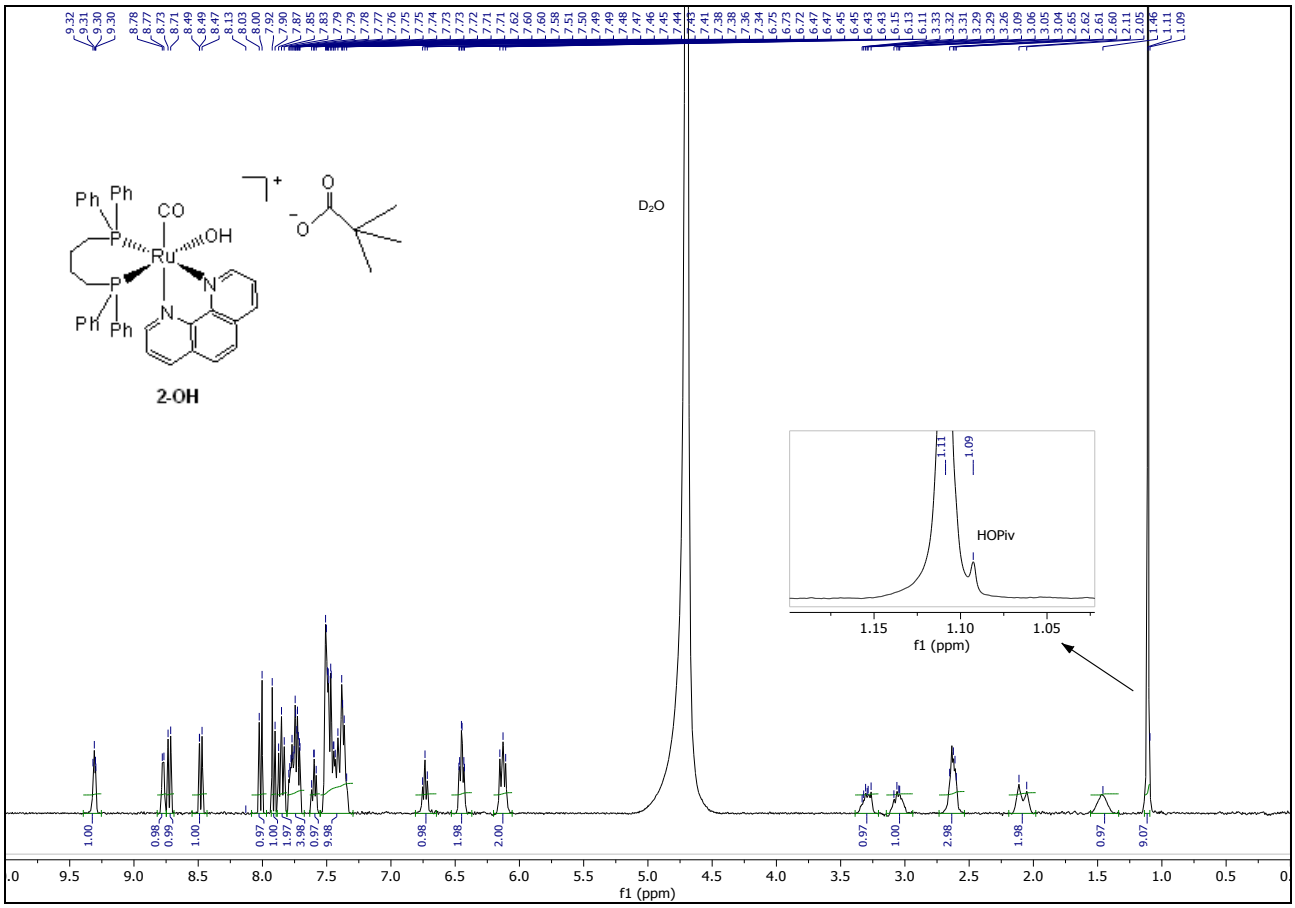

Figure S34. ^{1}H NMR spectrum (400.1 MHz) of [Ru(OPiv)(CO)(dppb)(phen)]OPiv (**2**) in D_2O at 298 K.

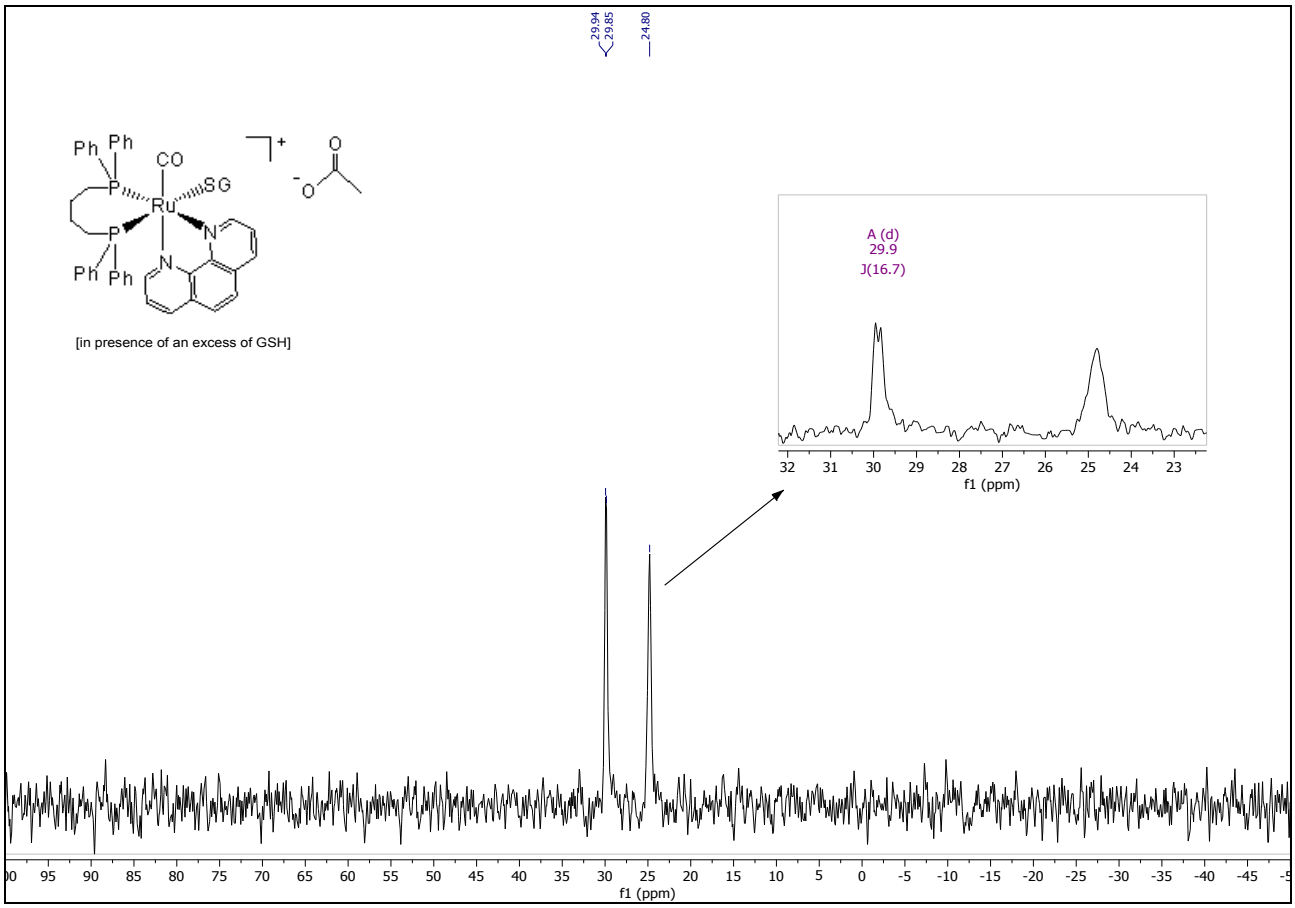

Figure S35. $^{31}P\{^{1}H\}$ NMR spectrum (162 MHz) of the products of the reaction between [Ru(OPiv)(CO)(dppb)(phen)]OPiv (**2**) and GSH (2 equiv) in D_2O at 298 K.

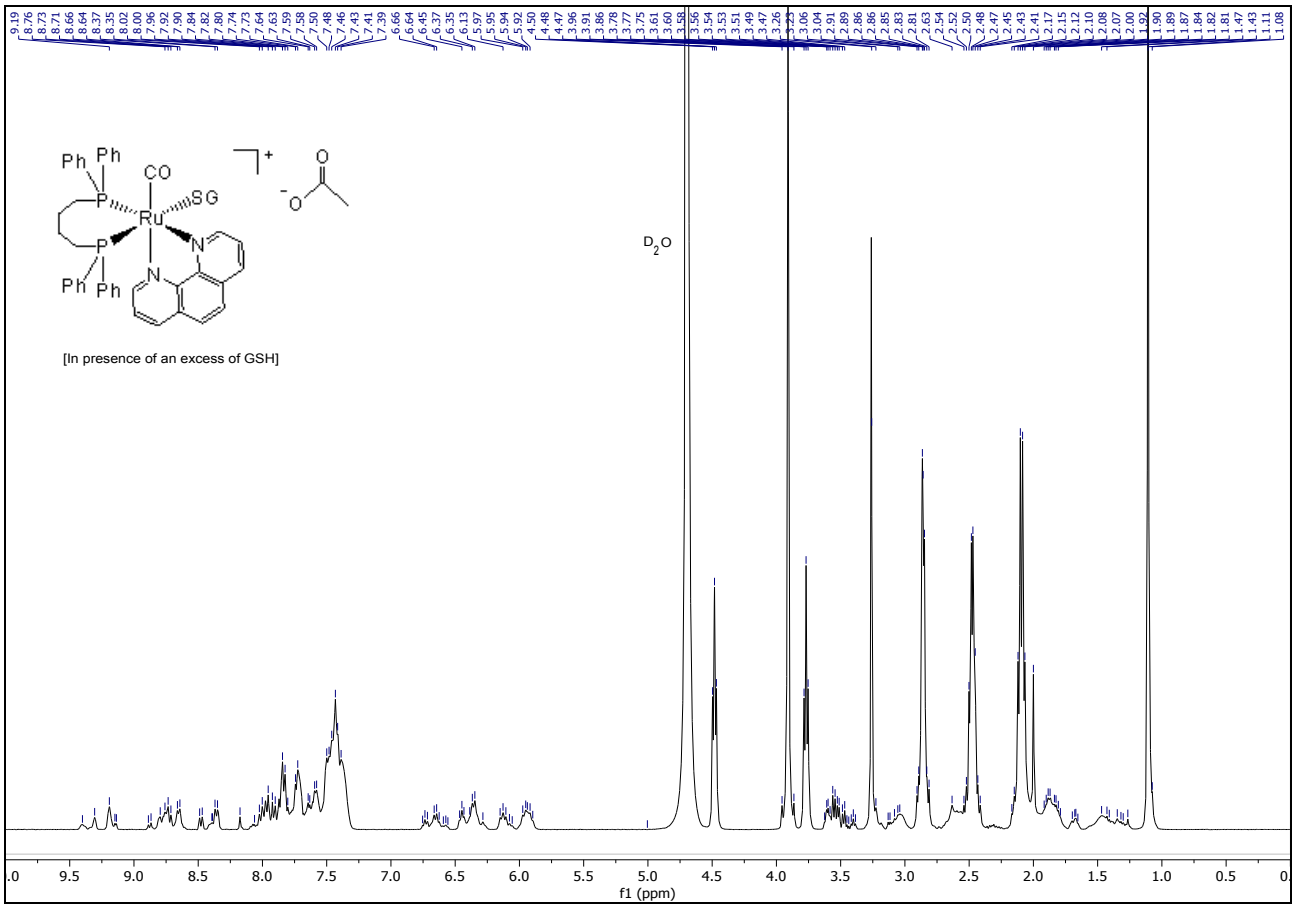

Figure S36. ^{1}H NMR spectrum (400.1 MHz) of the products of the reaction between [Ru(OPiv)(CO)(dppb)(phen)]OPiv (**2**) and GSH (2 equiv) in D_2O at 298 K.

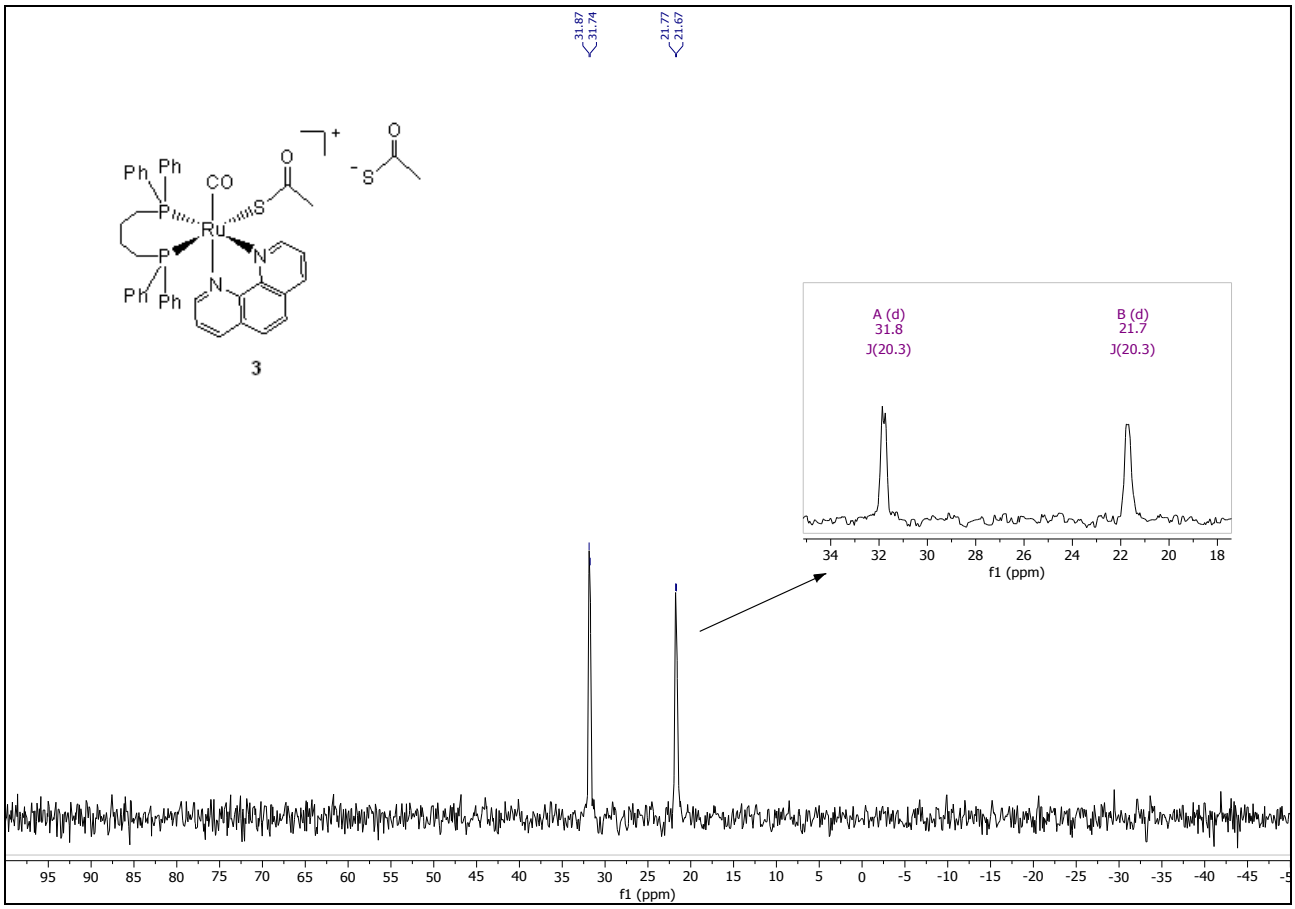

Figure S37. $^{31}P\{^{1}H\}$ NMR spectrum (162 MHz) of [Ru(SAc)(CO)(dppb)(phen)]SAc (**3**) in DMSO-d_6 at 298 K after 48 h.

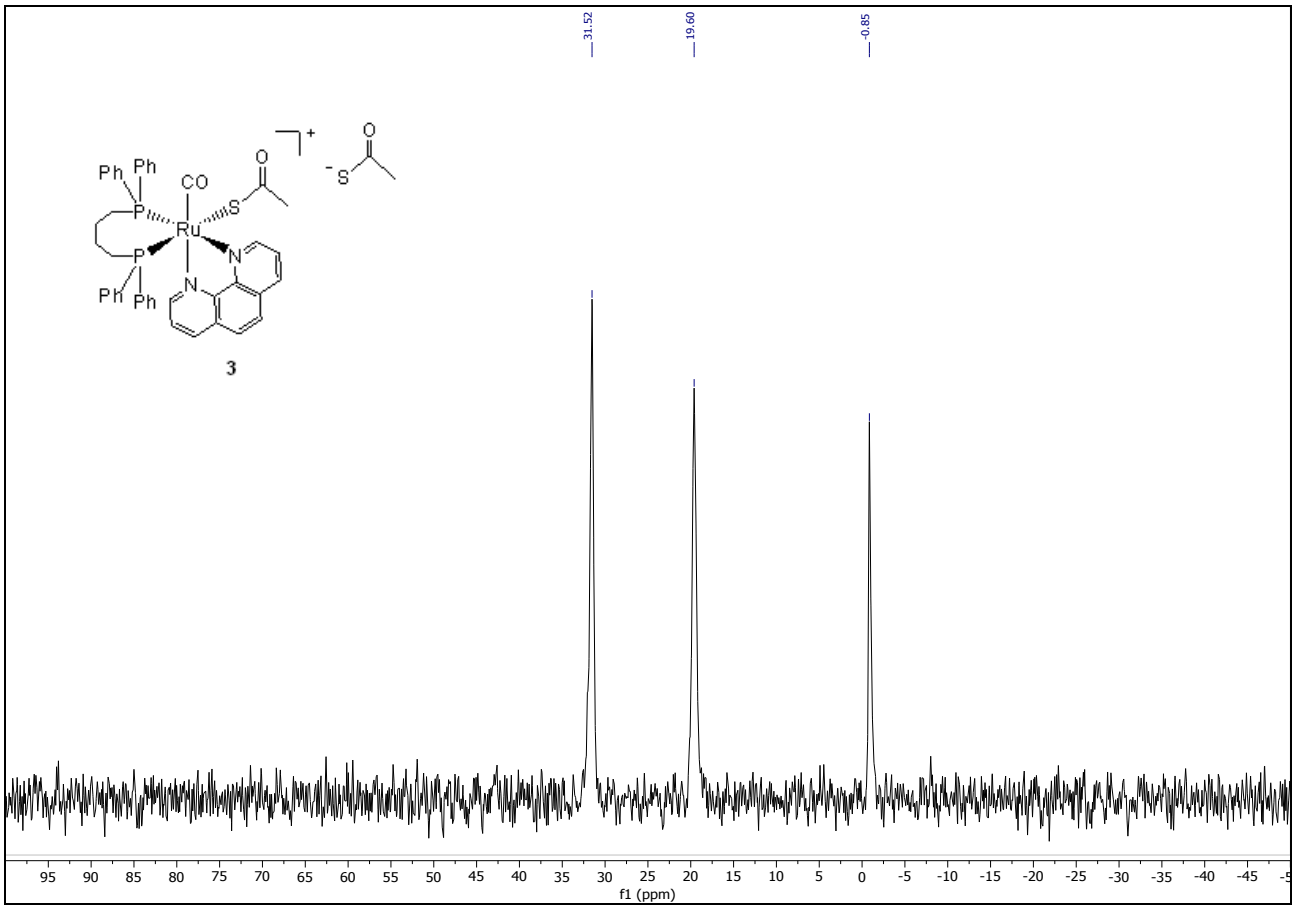

Figure S38. $^{31}P\{^{1}H\}$ NMR spectrum (162 MHz) of [Ru(SAc)(CO)(dppb)(phen)]SAc (**3**) in a DMSO-d_6/RPMI 1640 medium mixture (1:1 (v/v)) at 298 K after 48 h.

Single crystal X-Ray structure determination of compounds 1 and 4.

General data.

Data were collected on a single crystal x-ray diffractometer equipped with a CMOS detector (Bruker APEX III, κ-CMOS), a TXS rotating anode with MoK_α radiation (λ = 0.71073 Å) and a Helios optic using the APEX3 software package.[1] Measurements were performed on single crystals coated with perfluorinated ether. The crystals were fixed on top of a kapton micro sampler and frozen under a stream of cold nitrogen. A matrix scan was used to determine the initial lattice parameters. Reflections were corrected for Lorentz and polarisation effects, scan speed, and background using SAINT.[2] Absorption correction, including odd and even ordered spherical harmonics was performed using SADABS.[3] Space group assignment was based upon systematic absences, E statistics, and successful refinement of the structures. The structures were solved using SHELXT with the aid of successive difference Fourier maps, and were refined against all data using SHELXL in conjunction with SHELXLE.[4,5,6] Hydrogen atoms were calculated in ideal positions as follows: Methyl hydrogen atoms were refined as part of rigid rotating groups with a C–H distance of 0.98 Å and $U_{iso(H)}$ = 1.5·$U_{eq(C)}$. Other H atoms were placed in calculated positions and refined using a riding model, with methylene and aromatic C–H distances of 0.99 Å and 0.95 Å, respectively, and other C–H distances of 1.00 Å, all with $U_{iso(H)}$ = 1.2·$U_{eq(C)}$. Non-hydrogen atoms were refined with anisotropic displacement parameters. Full-matrix least-squares refinements were carried out by minimizing $\Sigma w(F_o^2 - F_c^2)^2$ with the SHELXL weighting scheme.[5] Neutral atom scattering factors for all atoms and anomalous dispersion corrections for the non-hydrogen atoms were taken from *International Tables for Crystallography*.[7] A split layer refinement was used for disordered groups and additional restraints on geometries and anisotropic displacement parameters were used, if necessary. The unit cell of **1** contains 8 disordered molecules of water and the unit cell of **4** contains a mixture of disordered solvents which were treated as a diffuse contribution to the overall scattering without specific atom positions using the PLATON/SQUEEZE procedure.[8] Images of the crystal structures were generated with Mercury.[9] CCDC 1995146-1995147 contains the supplementary crystallographic data for this paper. These data are provided free of charge by The Cambridge Crystallographic Data Centre.

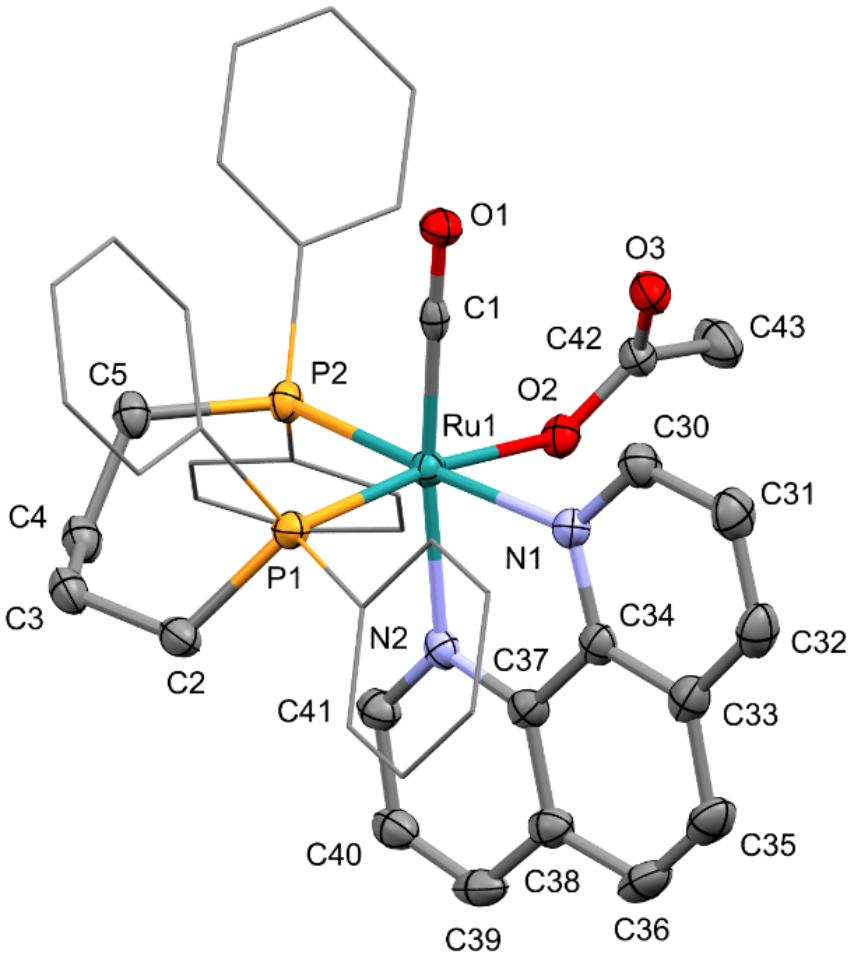

Figure S39. Molecular structure of complex **1** (CCDC 1995146) as determined by single crystal X-ray diffraction. Ellipsoids are displayed at the 50% probability level, hydrogen atoms as well as the OAc counterion are omitted, and phenyl groups are simplified as wireframes for clarity.

Single Crystal X-Ray Structure Determination of Compound 1 (CCDC 1995146).

Detailed Crystallographic Data.

Diffractometer operator:	C. Jandl
Scanspeed	1-10 s per frame
Dx	37 mm
Frames:	2690 measured in 12 data sets
phi-scans with delta phi	0.5
omega-scans with delta omega	0.5
shutterless mode	

Crystal Data:

Compound	[Ru(OAc)(CO)(dppb)(phen)]OAc (**1**)	
Chemical formula of the crystal	$[C_{43}H_{39}N_2O_3P_2Ru \cdot C_2H_3O_2 \cdot O]$	
Formula weight (M_r)	869.82	
Temperature	100 K	
Mo $K\alpha$ radiation	λ = 0.71073 Å	
Crystal habit	Fragment, colorless	
Crystal size	0.16 × 0.11 × 0.05 mm	
Crystal system	Triclinic, *P*	
Hall symbol	-P 1	
Cell parameters from 9906 reflections:		
θ	2.2-25.8°	
μ	0.49 mm^{-1}	
Unit cell dimensions	a = 11.628(3) Å	α = 105.674(7)°
	b = 11.773(3) Å	β = 103.463(7)°
	c = 17.460(4) Å	γ = 102.418(7)°
Volume	2137.2(9) $Å^3$	
Z	2	
Density (calculated)	1.352 g/cm^3	
F(000)	896	

Data collection:

Diffractometer	Bruker Photon CMOS
Radiation source	TXS rotating anode, Mo
Helios optic monochromator	
Detector resolution	16 pixels mm^{-1}
phi- and ω-rotation scans	
Absorption correction	Multi-Scan *SADABS* 2016/2, Bruker
	T_{min} = 0.685, T_{max} = 0.745
Theta range for data collection	θ_{max} = 25.4°, θ_{min} = 1.9°
Index ranges	$-14 \leq h \leq 14$, $-14 \leq k \leq 14$, $-21 \leq l \leq 21$
Reflections collected	77583
Independent reflections	7805
Reflections with $I > 2\sigma(I)$	6393
R(int)	0.090

Structure refinement:

Refinement on F^2	
Least-squares matrix	full
$R[F^2 > 2\sigma(F^2)]$	0.040
$wR(F^2)$	0.103
S	1.10
Reflections / restraints / parameters	7805 / 156 / 554
Constraints	0
Primary atom site location	intrinsic phasing
Secondary atom site location	difference Fourier map
Hydrogen site location	inferred from neighboring sites
H-atom parameters constrained	
Weighting scheme	$w = 1/[\Sigma^2(F_o^2) + (0.038P)^2 + 3.7383P]$
	where $P = (F_o^2 + 2F_c^2)/3$
$(\Delta/\sigma)_{max}$	0.001
$\Delta\rho_{max}$	0.86 $eÅ^{-3}$
$\Delta\rho_{min}$	-0.67 $eÅ^{-3}$

Extinction correction	none
Extinction coefficient	-

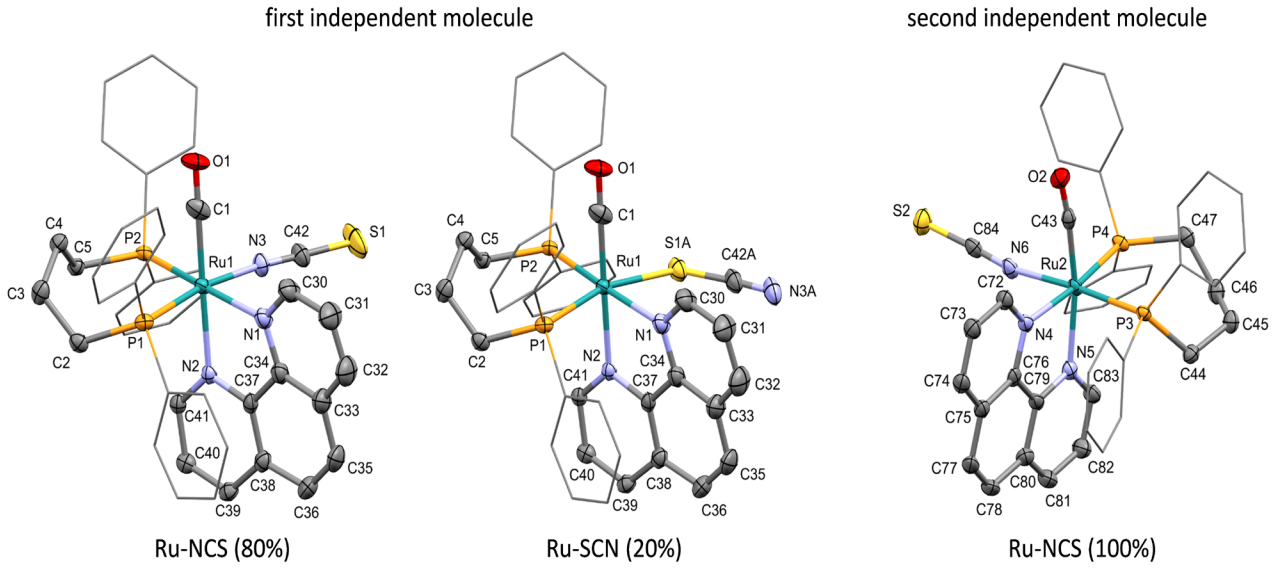

Figure S40. Molecular structure of complex **4** (CCDC 1995147) in the solid state; left and center: First independent molecule in the asymmetric unit showing the disordered Ru-NCS (ca. 80%) and Ru-SCN (ca. 20%) binding isomers; right: second independent molecule, exhibiting only the Ru-NCS isomer. Ellipsoids are displayed at the 50% probability level, hydrogen atoms as well as the SCN counterions and additional disorder are omitted, and phenyl groups are simplified as wireframes for clarity.

Single Crystal X-Ray Structure Determination of Compound 4 (CCDC 1995147).

Detailed Crystallographic Data.

Diffractometer operator:	C. Jandl
Scanspeed	2-20 s per frame
Dx	40 mm
Frames:	3480 measured in 13 data sets
phi-scans with delta phi	0.5
omega-scans with delta omega	0.5
shutterless mode	

Crystal Data:

Compound	[Ru(NCS)(CO)(dppb)(phen)]SCN (**4**)	
Chemical formula of the crystal	$[C_{42}H_{36}N_3OP_2RuS \cdot CNS]$	
Formula weight (M_r)	851.86	
Temperature	100 K	
Mo $K\alpha$ radiation	λ = 0.71073 Å	
Crystal habit	Fragment, yellow	
Crystal size	0.19 × 0.17 × 0.11 mm	
Crystal system	Triclinic, *P*	
Hall symbol	-P 1	
Cell parameters from 9210 reflections:		
θ	2.2-26.5°	
μ	0.62 mm^{-1}	
Unit cell dimensions	a = 14.9335(9) Å	α = 80.178(2)°
	b = 15.2819(9) Å	β = 67.601(2)°
	c = 19.0590(12) Å	γ = 83.202(2)°
Volume	3955.6(4) $Å^3$	
Z	4	
Density (calculated)	1.430 g/cm^3	
F(000)	1744	

Data collection:

Diffractometer	Bruker Photon CMOS
Radiation source	TXS rotating anode
Helios optic monochromator	
Detector resolution	16 pixels mm^{-1}
phi- and ω-rotation scans	
Absorption correction	Multi-Scan *SADABS* 2016/2, Bruker
	T_{min} = 0.725, T_{max} = 0.745
Theta range for data collection	θ_{max} = 25.4°, θ_{min} = 2.3°
Index ranges	$-17 \leq h \leq 17$, $-18 \leq k \leq 18$, $-22 \leq l \leq 22$
Reflections collected	210209
Independent reflections	14460
Reflections with $I > 2\sigma(I)$	12991
R(int)	0.035

Structure refinement:

Refinement on F^2	
Least-squares matrix	full
$R[F^2 > 2\sigma(F^2)]$	0.029
$wR(F^2)$	0.081
S	1.08
Reflections / restraints / parameters	14460 / 1232 / 1242
Constraints	0
Primary atom site location	intrinsic phasing
Secondary atom site location	difference Fourier map
Hydrogen site location	inferred from neighboring sites
H-atom parameters constrained	
Weighting scheme	$w = 1/[\Sigma^2(F_o^2) + (0.0352P)^2 + 6.105P]$
	where $P = (F_o^2 + 2F_c^2)/3$
$(\Delta/\sigma)_{max}$	0.023
$\Delta\rho_{max}$	1.03 $eÅ^{-3}$
$\Delta\rho_{min}$	-1.19 $eÅ^{-3}$

Extinction correction	none
Extinction coefficient	-

Coordination Mode of the Thiocyanate Ligand in Complex 4

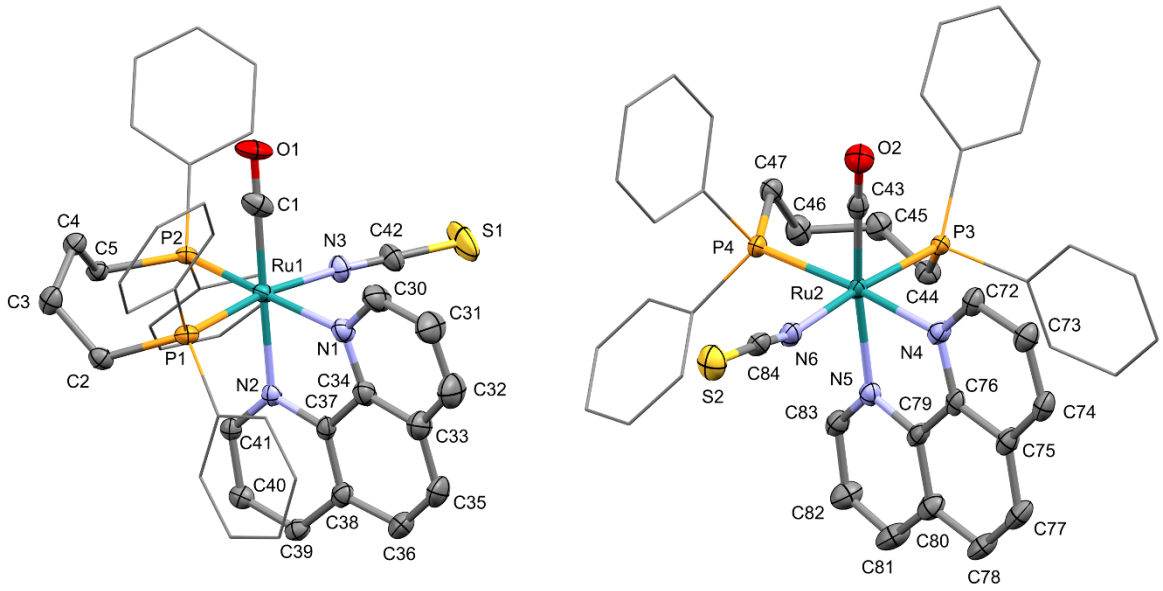

Figure S41. Molecular structure of both crystallographically independent molecules from the crystal structure of compound **4** (left: Ru-NCS isomer of the first independent molecule, right: second independent molecule). Ellipsoids are displayed at the 50% probability level, hydrogen atoms as well as counterions and disorder are omitted, and phenyl groups are simplified as wireframes for clarity.

As stated in the main manuscript, the binding mode of the NCS ligand is not uniform across the two independent molecules in the crystal structure of compound **4**. In the second molecule (Figure S41, right) the binding mode is exclusively via N without any disorder or ambiguities. In the first molecule (Figure S41, left) the NCS ligand is heavily disordered alongside with a minor disorder of the neighboring CO ligand. A successful model could be found involving three NCS residues (with an altogether occupancy of ca. 80%) coordinating via N in a similar fashion to the non-disordered molecule and two NCS residues (with a combined occupancy of ca. 20%) coordinating via S (see Figure S42). While the N-binding mode only moderately deviates from linearity, the S-binding mode is strongly bent, although the high degree of disorder does not allow the determination of exact binding angles. Despite these uncertainties the coordination geometries are in reasonable agreement with literature-reported crystal structures, where the N-binding mode to Ru is also more common than the S-binding mode, of which only a handful of examples is reported.[10] Further differences between the two molecules involve the conformation of the dppb ligand, the alkyl bridge of which is oriented in the direction of the CO ligand in the first molecule ("upwards" in Figure S41, left), but twisted in the other direction in the second molecule (same as in the structure of **1**). This causes a different orientation of the phenyl groups, so the π-π-interaction occurs between a phenyl group and

an outer aromatic ring of phenanthroline in the first molecule, whereas in the second molecule the π-π-stacking involves the central phenanthroline ring in analogy to the structure of **1**. This difference is also reflected in the different Ru-P bond lengths (2.3762(7) Å and 2.3695(7) Å for the first molecule; 2.3385(7) Å and 2.3460(7) Å for the second molecule) and bite angles of the dppb ligand (100.24(3)° for the first molecule, 94.79(2)° for the second molecule). It can be assumed that the different surrounding caused by this change in conformation allows for the co-crystallization of the species with the alternate binding mode via S of the NCS ligand in the solid state.

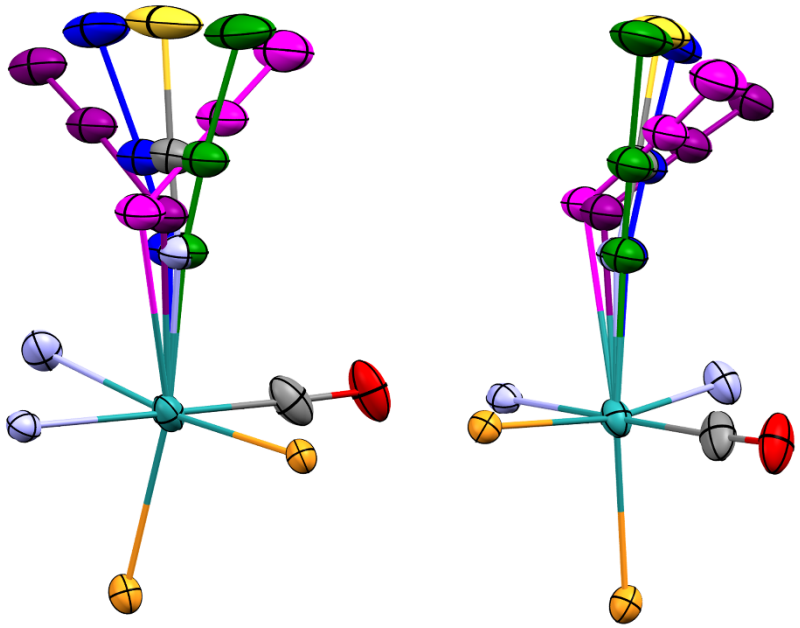

Figure S42. Two perspectives of the coordination environment of the Ru center bearing the disordered NCS ligand in compound **4**. Ellipsoids are displayed at the 50% probability level. Color code: Ru (turquoise), O (red), N (light blue), C (grey), P (orange), S (yellow). The main NCS residue (occupancy 59%) is drawn in normal colors, other residues binding via N in green (7%) and blue (12%), residues binding via S in magenta (14%) and violet (8%).

Table S1. Effects of complexes **1-5** and Cisplatin in ATC cell viability after 48 h treatment in SW1736 cells.

Complexes	0,5 µM	1 µM	2 µM	2,5 µM	5 µM
1	0,86	0,78	0,52	0,37	0,24
2	0,53	0,39	0,36	0,12	0,02
3	0,38	0,28	0,14	0,01	0,01
4	1,04	1,06	0,74	0,61	0,35
5	1,01	0,80	0,51	0,42	0,38
cisplatin	0,93	0,91	0,88	0,74	0,67

For each complex and concentration, percentage of control is listed in the table. For each cell viability value, the standard deviation is below 10%.

Table S2. Effects of complexes **1-5** and Cisplatin in ATC cell viability after 72 h treatment in SW1736 cells.

Complexes	0,5 µM	1 µM	2 µM	2,5 µM	5 µM
1	0,73	0,60	0,35	0,25	0,16
2	0,41	0,28	0,26	0,16	0,10
3	0,24	0,17	0,06	0,01	0,00
4	0,97	0,90	0,65	0,53	0,32
5	0,95	0,75	0,54	0,52	0,28
cisplatin	0,92	0,88	0,81	0,74	0,52

For each complex and concentration, percentage of control is listed in the table. For each cell viability value, the standard deviation is below 10%.

Table S3. Effects of complexes **1-5** and Cisplatin in ATC cell viability after 48 h treatment in 8505C cells.

Complexes	0,5 µM	1 µM	2 µM	2,5 µM	5 µM
1	0,98	0,88	0,48	0,36	0,18
2	0,72	0,53	0,45	0,28	0,13
3	0,49	0,36	0,20	0,14	0,12
4	1,10	1,04	0,75	0,42	0,21
5	1,04	0,82	0,53	0,51	0,33
cisplatin	0,92	0,94	0,85	0,88	0,64

For each complex and concentration, percentage of control is listed in the table. For each cell viability value, the standard deviation is below 10%.

Table S4. Effects of complexes **1-5** and Cisplatin in ATC cell viability after 72 h treatment in 8505C cells.

Complexes	0,5 µM	1 µM	2 µM	2,5 µM	5 µM
1	1,02	1,04	0,58	0,36	0,23
2	0,38	0,16	0,17	0,12	0,09
3	0,21	0,15	0,12	0,09	0,01
4	0,86	0,75	0,59	0,53	0,38
5	0,94	0,70	0,46	0,32	0,22
cisplatin	0,91	0,88	0,78	0,66	0,47

For each complex and concentration, percentage of control is listed in the table. For each cell viability value, the standard deviation is below 10%.

References.

(1) *APEX suite of crystallographic software*, APEX 3, Version 2015.5-2, Bruker AXS Inc., Madison, Wisconsin, USA, 2015.

(2) *SAINT*, Version 8.38A, Bruker AXS Inc., Madison, Wisconsin, USA, 2017.

(3) *SADABS*, Version 2016/2, Bruker AXS Inc., Madison, Wisconsin, USA, 2016.

(4) G. M. Sheldrick, *Acta Crystallogr. Sect. A* **2015**, *71*, 3-8.

(5) G. M. Sheldrick, *Acta Crystallogr. Sect. C* **2015**, *71*, 3-8.

(6) C. B. Hübschle, G. M. Sheldrick, B. Dittrich, *J. Appl. Cryst.* **2011**, *44*, 1281-1284.

(7) *International Tables for Crystallography, Vol. C* (Ed.: A. J. Wilson), Kluwer Academic Publishers, Dordrecht, The Netherlands, **1992**, Tables 6.1.1.4 (pp. 500-502), 4.2.6.8 (pp. 219-222), and 4.2.4.2 (pp. 193-199).

(8) A. L. Spek, *Acta Crystallogr. Sect. C* **2015**, *71*, 9–18.

(9) C. F. Macrae, I. J. Bruno, J. A. Chisholm, P. R. Edgington, P. McCabe, E. Pidcock, L. Rodriguez-Monge, R. Taylor, J. van de Streek, P. A. Wood, *J. Appl. Cryst.* **2008**, *41*, 466-470.

(10) C. R. Groom, I. J. Bruno, M. P. Lightfoot, S. C. Ward, *Acta Crystallogr. Sect B*, **2016**, *72*, 171-179.